

A Global Treatment Of VMD Physics Up To The ϕ :

I. e^+e^- Annihilations, Anomalies And Vector Meson Partial Widths

M. Benayoun, P. David, L. DelBuono, O. Leitner

LPNHE Paris VI/VII, IN2P3/CNRS, F-75252 Paris, France

August 18, 2018

Abstract

The HLS Model, equipped with a mechanism providing the breaking of $U(3)/SU(3)$ symmetry and an isospin symmetry breaking leading naturally to vector meson mixing, has been recently shown to successfully account for $e^+e^- \rightarrow \pi^+\pi^-$ cross section and for the dipion spectrum in τ decay. The present study shows that the full anomalous sector of the HLS model can be considered and is validated by the experimental data. Indeed, this extended model provides a successful simultaneous fit to the $e^+e^- \rightarrow \pi^+\pi^-$ data together with the available data on $e^+e^- \rightarrow \pi^0\gamma$, $e^+e^- \rightarrow \eta\gamma$ and $e^+e^- \rightarrow \pi^0\pi^+\pi^-$ cross sections. It is shown that the fit of these data sets also predicts an accurate description of the $\eta/\eta' \rightarrow \pi^+\pi^-\gamma$ decays fully consistent with the reported information on their branching fractions and spectra. Finally, one also derives from our global fits products of widths of the form $\Gamma(V \rightarrow f_1)\Gamma(V \rightarrow e^+e^-)$ and ratios of the form $\Gamma(V \rightarrow f_1)/\Gamma(V \rightarrow f_2)$ describing decays of vector mesons to several non-leptonic final states.

1 Introduction

A Lagrangian model based on the Hidden Local Symmetry Model [1, 2] has been used [3] in order to account simultaneously for the $e^+e^- \rightarrow \pi^+\pi^-$ and $\tau^\pm \rightarrow \pi^\pm\pi^0\nu_\tau$ data. This model has been supplied with a SU(3)/U(3) symmetry breaking mechanism [4, 5], essentially relying on the BKY [6] mechanism. In order to apply this model simultaneously to annihilation data and to the $\pi\pi$ spectrum from τ decays, an isospin breaking mechanism has been defined, which is also a specific implementation of the vector meson mixing. This is needed at least in order to account for the $\omega \rightarrow \pi^+\pi^-$ decay which is an important signal in $e^+e^- \rightarrow \pi^+\pi^-$ data. Moreover, a global fit to e^+e^- and τ data needs a reasonably general isospin symmetry breaking mechanism, active in e^+e^- annihilations and which can be switched off for the τ decay.

The peculiar aspect of the mixing model defined in [3] is the use of several decay modes which serve to constrain the parameters introduced by these breaking schemes. Then, the anomalous decay modes of the form¹ $VP\gamma$ and the two photon decay widths of the π^0 , η , η' mesons play an important role.

As such, the model is already overconstrained and has been successfully used [3]. However, it cannot apply to e^+e^- annihilation channels other than $\pi^+\pi^-$, K^+K^- and $K^0\bar{K}^0$, and processes like $e^+e^- \rightarrow \pi^0\gamma$, $e^+e^- \rightarrow \eta\gamma$, $e^+e^- \rightarrow \eta'\gamma$ or $e^+e^- \rightarrow \pi^0\pi^+\pi^-$, remain beyond its scope. Indeed, even if $V \rightarrow P\gamma$ decay widths are an important part of these processes, they do not exhaust the physics content of the annihilation processes.

Therefore, having a model able to describe all these processes (and possibly others, as for instance $e^+e^- \rightarrow \pi^0\omega$) is certainly valuable. This is already important from a physics point of view but, more technically, this may allow to check the relative consistency of various data sets within the same framework and, therefore, the systematics affecting the data sets.

An extension of the HLS model is possible by introducing the anomalous Lagrangian pieces identified long ago [7, 2] and relying also on the above mentioned breaking schemes reminded or defined in [3]. This could allow interesting improvements in estimating the hadronic contribution to the muon anomalous magnetic moment a_μ . Indeed, as basically several crucial physics parameters are common to all low energy annihilations, considering all annihilation processes altogether may turn out to increase the statistics and, then, improve uncertainties. In this way, one may expect a better determination of $e^+e^- \rightarrow \pi^+\pi^-$ using all other annihilation processes. Conversely, the huge experimental effort invested in order to get accurate $e^+e^- \rightarrow \pi^+\pi^-$ data may help in better estimating contributions to a_μ from other processes, $e^+e^- \rightarrow \pi^0\pi^+\pi^-$ for instance. However, the systematics present in all these processes may limit the expected improvements.

The purpose of the present study is to construct such a model and test its ability to account for the above mentioned processes beside $e^+e^- \rightarrow \pi^+\pi^-$. This study will be split up into two parts for ease of reading. In the following, we will build the model and apply it to several annihilation processes and decay width information. An accompanying paper is devoted to analyzing the dipion spectra in τ decay and some non-perturbative contributions to a_μ .

¹ Throughout this paper, we denote by P and V , resp. the basic pseudoscalar and vector meson *nonets*. The explicit form of their matrix representation can be found in several papers [1, 2, 4, 5] and is reminded in [3]. The electromagnetic field is denoted by A . All definitions and notations in the present paper closely follow those in [3].

We leave aside from the present study the $e^+e^- \rightarrow K^+K^-/K^0\bar{K}^0$ annihilation channels which are known to raise a problem thoroughly examined in [8] and may call for a solution beyond the scope of effective Lagrangians [9]. Indeed, the ratio of the partial widths of ϕ decays to a charged or neutral kaon pair looks inconsistent with expectations. This question raises an issue which deserves a specific study at the level of cross sections which we have only started.

The paper is organized as follows. Section 2 reminds the ingredients to be used in order to construct the Lagrangian of our Extended Model : these can be found in [7, 2]. Without further constraints, this leads to introducing three more free parameters. In Section 3, we require these anomalous Lagrangians to recover identically amplitudes at the chiral limit as given by the standard Wess–Zumino–Witten (WZW) Lagrangians [10, 11] ; this leads to constraining some of the parameters above and, then, to reduce the additional parameter freedom of the model. In Sections 4 and 5, we briefly remind the isospin breaking model of [3], mostly in order to simplify notations. Section 6 is devoted to our treatment of correlated systematic errors which introduce uncertainties on the global scale of spectra ; we also emphasize the way to check the scale information provided with the various data sets. A method to account for possible data discrepancies is also given. In Section 7, the Extended Model is shown to keep intact the description of the $e^+e^- \rightarrow \pi^+\pi^-$ data examined in [3], together with the unavoidable set of 17 radiative and leptonic decays.

In Section 8 the real use of the Extended Model begins with fitting the $e^+e^- \rightarrow \pi^0\gamma$ and $e^+e^- \rightarrow \eta\gamma$ data simultaneously with our usual set of $e^+e^- \rightarrow \pi^+\pi^-$ data [3]. While introducing these data sets, one has to remove all $V\pi^0\gamma$ and $V\eta\gamma$ decay pieces of information from the set of decay partial widths used together with annihilations, in order to avoid redundancies. At this step, the new Lagrangian pieces are shown to correctly account for the data. In Section 9, one performs a fit of the $e^+e^- \rightarrow \pi^+\pi^-$ data collected by the KLOE Collaboration using the Initial State Radiation Method (ISR). This is seemingly the first published fit to the KLOE data [12, 13]. The next step, including the $e^+e^- \rightarrow \pi^0\pi^+\pi^-$ annihilation data in our fit procedure, is the subject of Section 10, where a discussion on the various data samples is done. In Section 11 numerical values for ω and ϕ meson parameters are given and the exact strength of the $APPP$ and $VPPP$ couplings is emphasized.

The aim of Section 12 is to show that the Extended Model, with parameters fixed by fitting to the cross section listed above, allows to accurately predict the properties (spectrum lineshape, partial width) of the decay channels $\eta/\eta' \rightarrow \pi^+\pi^-\gamma$, both dominated by the box anomalies of QCD. In Section 13, we focus on vector meson partial widths and discuss the question of getting their absolute values from e^+e^- data only, where models are sensitive – for each vector meson – to only the product of its leptonic decay width and of its partial width to the final state of the e^+e^- annihilation. Finally, a few concluding remarks are collected in the Conclusion to the present part. Some reminders or results are given in Appendices, in order to keep the main text as clear as possible.

2 The Extended HLS Lagrangian Model

The most general Lagrangian of the HLS model [1, 2, 7] involves anomalous and non-anomalous sectors. It can be written :

$$\mathcal{L} = \mathcal{L}_{HLS} + \mathcal{L}_{YM} + \mathcal{L}_{WZW} + \mathcal{L}_{FKTUY} \quad (1)$$

The piece denoted \mathcal{L}_{HLS} can be written $\mathcal{L}_A + a\mathcal{L}_V$, where a is the specific HLS parameter, expected equal to 2 if vector dominance is fully satisfied. This Lagrangian piece allows a direct coupling of photons to pseudoscalar mesons to survive with a magnitude proportional to $a - 2$. This piece, which accounts for the non-anomalous sector, has been given in expanded form in [4]. A brief survey of the HLS model can be found in Appendix A of [3] and is enough for the purpose of the present paper. A recent and comprehensive review can be found in [2], for instance.

The parts of the HLS Lagrangian \mathcal{L}_{HLS} specific of the e^+e^- physics (\mathcal{L}_{VMD}) and τ decays (\mathcal{L}_τ) have also been given in [3] ; they are reproduced with almost no comment in the Appendix (see Section A) in order to avoid too frequent references to an external paper.

\mathcal{L}_{YM} is the Yang–Mills piece which accounts for the vector mesons and exhibits the non-abelian group structure of the vector fields (see Eq. (D.1) in [3]).

\mathcal{L}_{WZW} and \mathcal{L}_{FKTUY} are the anomalous Wess–Zumino–Witten [10, 11] and FKTUY [7, 2] Lagrangian pieces which account for parity violating decays. Very briefly, the anomalous Lagrangian can be formally written :

$$\mathcal{L}_{anomalous} = \mathcal{L}_{WZW} + \sum_{i=1}^4 c_i \mathcal{L}_i \quad (2)$$

where the c_i 's are arbitrary constants weighting the additional FKTUY anomalous Lagrangians. Limiting oneself to the photon and vector meson couplings, $\mathcal{L}_{anomalous}$ can be cast in the form[2] :

$$\mathcal{L}_{anomalous} = \mathcal{L}_{VVP} + \mathcal{L}_{AVP} + \mathcal{L}_{AAP} + \mathcal{L}_{VPPP} + \mathcal{L}_{APPP} \quad (3)$$

where A denotes the electromagnetic field. The Lagrangian pieces occurring in Eq. (3) are² [2] :

$$\left\{ \begin{array}{l} \mathcal{L}_{VVP} = -\frac{N_c g^2}{4\pi^2 f_\pi} c_3 \epsilon^{\mu\nu\alpha\beta} \text{Tr}[\partial_\mu V_\nu \partial_\alpha V_\beta P] \\ \mathcal{L}_{AVP} = -\frac{N_c g e}{8\pi^2 f_\pi} (c_3 - c_4) \epsilon^{\mu\nu\alpha\beta} \partial_\mu A_\nu \text{Tr}[\{\partial_\alpha V_\beta, Q\} P] \\ \mathcal{L}_{AAP} = -\frac{N_c e^2}{4\pi^2 f_\pi} (1 - c_4) \epsilon^{\mu\nu\alpha\beta} \partial_\mu A_\nu \partial_\alpha A_\beta \text{Tr}[Q^2 P] \\ \mathcal{L}_{VPPP} = -i \frac{N_c g}{4\pi^2 f_\pi^3} (c_1 - c_2 - c_3) \epsilon^{\mu\nu\alpha\beta} \text{Tr}[V_\mu \partial_\nu P \partial_\alpha P \partial_\beta P] \\ \mathcal{L}_{APPP} = -i \frac{N_c e}{3\pi^2 f_\pi^3} \left[1 - \frac{3}{4}(c_1 - c_2 + c_4)\right] \epsilon^{\mu\nu\alpha\beta} A_\mu \text{Tr}[Q \partial_\nu P \partial_\alpha P \partial_\beta P] \end{array} \right. \quad (4)$$

²For clarity, the new constant parameters are denoted exactly as they are defined in [2].

where we have extracted the universal vector meson coupling constant g from the definition of the vector field matrix (see [3] for our definitions), Q denotes the quark charge matrix and $\{\partial_\alpha V_\beta, Q\}$ is the anticommutator of its arguments. N_c is the number of quark colors, 3 in our case. The original WZW terms here can be easily identified in Eqs (4) and one also observes that these Lagrangians depend on only 3 (FKTUY) parameter combinations : $c_1 - c_2$, c_3 and c_4 . We may refer to the first three Lagrangians in Eqs. (4) as Triangle Anomaly and the last two as Box Anomaly Lagrangians.

If full Vector Meson Dominance were fulfilled, one would have :

$$c_3 = c_4 = 1 \quad \text{and} \quad c_1 - c_2 = \frac{1}{3} \quad . \quad (5)$$

Indeed, one can easily check that these conditions turn out to cancel the 3 Lagrangian pieces in Eqs. (4) involving the photon field (A). In this case, photons connect to hadrons only through the $V - A$ transitions allowed by the non-anomalous HLS Lagrangian (see Appendix A).

However, relying on a limited subset of data, it has been argued in [7, 2] that some experimental data may instead favor :

$$c_3 = c_4 = c_1 - c_2 = 1 \quad (6)$$

Previous studies especially devoted to $VP\gamma$ and $P\gamma\gamma$ partial widths [5] performed assuming Eqs. (6) were successful enough to conclude that these conditions were well accepted by the data. Our work [14] on a simultaneous account of $\eta/\eta' \rightarrow \gamma\gamma$ and $\eta/\eta' \rightarrow \pi^+\pi^-\gamma$ led to the same conclusion. This gave a strong support to the relevance of the box anomaly phenomenon in pseudoscalar meson decays.

Therefore, the present status is that full VMD is well accepted by all existing data only in the Triangle Anomaly sector, while the $\eta/\eta' \rightarrow \pi^+\pi^-\gamma$ decay modes prevent extending full VMD to the Box Anomaly sector.

However, the statement $c_3 = c_4 = c_1 - c_2 = 1$ cannot be considered as firmly established without being motivated by a detailed study of all relevant data. If any, such a conclusion should only follow from a study involving the annihilation processes $e^+e^- \rightarrow \pi^0\gamma, \eta\gamma, \eta'\gamma, \pi^+\pi^-\pi^0$ in their full intricacy, beside the properties of the decay modes $\eta/\eta' \rightarrow \gamma\gamma$ and $\eta/\eta' \rightarrow \pi^+\pi^-\gamma$. As anomalous transitions also involve non-anomalous pieces, the data set to examine should certainly include the $e^+e^- \rightarrow \pi^+\pi^-$ annihilation process in order to define precisely the other model parameters.

Whether such a program is realistic and can be practically worked out is the subject of the present paper. It implies to go much beyond what has been done recently in [3] and formerly in studies devoted to radiative decays, our [5, 14] for instance.

3 U(3)/SU(3) Breaking And The WZW Conditions

We will not rediscuss here the U(3)/SU(3) breaking conditions in the non-anomalous sector which have been extensively discussed in our [4, 3] following the idea of Bando, Kugo and Yamawaki [6], referred to as BKY mechanism. A detailed summary of the U(3)/SU(3) (BKY)

breaking scheme is given in Appendix C of [3] where the corresponding breaking for the Yang–Mills piece has been also considered (see Appendix D herein). Let us only remind that the pseudoscalar bare field matrix P ($= P_8 + P_0$) undergoes a renormalization to P' :

$$\begin{cases} P' \equiv P'_8 + xP'_0 = X_A^{1/2}(P_8 + P_0)X_A^{1/2} \\ X_A = \text{Diag}(1, 1, z_A) \end{cases} \quad (7)$$

where $x \neq 1$ carries the (U(3)) nonet symmetry breaking³. The other breaking parameter has a well defined expression in terms of the kaon and pion decay constants : $z_A = [f_K/f_\pi]^2$. Correspondingly, the renormalized vector field matrix V' is given in terms of the bare one V [3] by :

$$\begin{cases} V'_\mu = X_T^{1/2}V_\mu X_T^{1/2} \\ X_T = \text{Diag}(1, 1, z_T) \end{cases} \quad (8)$$

Considering a HLS Lagrangian as general as allowed from its derivation [7, 2] leads to introduce *a priori* three more basic parameters ($c_1 - c_2, c_3$ and c_4) beside the standard g, a (and e) occurring already in the non–anomalous Lagrangian.

However, one may impose a natural constraint to this Extended HLS Model by requesting that it provides amplitudes identical to those derived from the WZW Lagrangian alone at the chiral point. These amplitudes may only be modified by U(3)/SU(3) breaking effects affecting the pseudoscalar sector [5, 3]. Instead, additional SU(3) breaking effects which may affect the trace terms in Eqs. (4), as well as the dependence upon the c_i 's, should drop out at the chiral point.

We perform the SU(3) breaking of each Lagrangian in Eqs. (4) using a prescription inspired from Bramon, Grau and Pancheri [17, 18]. This motivates the following breaking scheme :

$$\begin{cases} \mathcal{L}_{VVP} : \quad \text{Tr}[\partial_\mu V_\nu \partial_\alpha V_\beta P] \implies \text{Tr}[\partial_\mu V_\nu X_W \partial_\alpha V_\beta P] \\ \mathcal{L}_{AVP} : \quad \partial_\mu A_\nu \text{Tr}[\{\partial_\alpha V_\beta, Q\}P] \implies \partial_\mu A_\nu \text{Tr}[\{\partial_\alpha V_\beta, QX_U\}P] \\ \mathcal{L}_{AAP} : \quad \partial_\mu A_\nu \partial_\alpha A_\beta \text{Tr}[Q^2 P] \implies \partial_\mu A_\nu \partial_\alpha A_\beta \text{Tr}[X_R Q^2 P] \\ \mathcal{L}_{VPPP} : \quad \text{Tr}[V_\mu \partial_\nu P \partial_\alpha P \partial_\beta P] \implies \text{Tr}[X_K V_\mu \partial_\nu P \partial_\alpha P \partial_\beta P] \\ \mathcal{L}_{APPP} : \quad A_\mu \text{Tr}[Q \partial_\nu P \partial_\alpha P \partial_\beta P] \implies \text{Tr}[X_L Q \partial_\nu P \partial_\alpha P \partial_\beta P] \end{cases} \quad (9)$$

This might introduce as many as 5 more (breaking) parameters (z_W, z_U, z_R, z_K, z_L) as the five matrices introduced here are supposed to carry the same form than X_A or X_T reminded above. We now show that, actually, it is not the case.

3.1 The Triangle Anomaly Sector

Using the Lagrangians in Eqs. (4) broken as shown in Eqs. (9) just above and the $\gamma - V$ transition amplitudes as given by the non–anomalous Lagrangian, one can derive the ampli-

³See [15] for the relation between this parameter and determinant terms [16] explicitly breaking the $U_A(1)$ symmetry.

tudes :

$$T_X = T(X \rightarrow \gamma\gamma) \epsilon^{\mu\nu\alpha\beta} q_\mu^1 q_\nu^2 \epsilon_\alpha^1 \epsilon_\beta^2 \quad , \quad (X = \pi^0, \eta, \eta') \quad (10)$$

One gets first :

$$T(\pi^0 \rightarrow \gamma\gamma) = -i \frac{\alpha}{\pi f_\pi} [1 + 2(c_3 - c_4)] \quad (11)$$

which implies $c_3 = c_4$ in order to recover the usual WZW term. Therefore, the \mathcal{L}_{AVP} Lagrangian vanishes. Using this condition, one similarly derives :

$$\left\{ \begin{array}{l} T(\eta_0 \rightarrow \gamma\gamma) = -x \frac{i\alpha}{\pi f_\pi} \sqrt{\frac{2}{3}} \left[\frac{(1 - c_3)(z_W z_T^2 - z_R)}{3z_A} + \frac{z_W z_T^2 + 5z_A}{3z_A} \right] \\ T(\eta_8 \rightarrow \gamma\gamma) = -\frac{i\alpha}{\pi f_\pi} \sqrt{\frac{1}{3}} \left[\frac{-2(1 - c_3)(z_W z_T^2 - z_R)}{3z_A} + \frac{5z_A - 2z_W z_T^2}{3z_A} \right] \end{array} \right. \quad (12)$$

for the singlet and octet parts of the η and η' mesons. In order to recover the usual WZW expressions (see for instance [5, 14] or more recently [3]), one clearly needs to request $z_W z_T^2 = 1$, which was first phenomenologically found as a numerical constraint arising from fits [5]. If, additionally, one requests $z_R = 1$ (which may look quite natural), then the standard WZW amplitudes for $\eta_{0/8} \rightarrow \gamma\gamma$ are recovered without requiring any further constraint on c_3 . We are thus led to choose as constraints on the parameters :

$$z_W z_T^2 = z_R = 1 \quad , \quad c_3 = c_4 \quad (13)$$

3.2 The Box Anomaly Sector

As measurements related with box anomalies only involve couplings of the form $X\pi^+\pi^-\gamma$ with $X = \pi^0, \eta, \eta'$, we only focus on this sector. Let us list the Lagrangian pieces relevant for this purpose.

- A part only of the VVP Lagrangian plays a role in these couplings :

$$\left\{ \begin{array}{l} \mathcal{L}_{VVP} = C \epsilon^{\mu\nu\alpha\beta} \left\{ [\partial_\mu \rho_\nu^I \partial_\alpha \rho_\beta^I + \partial_\mu \omega_\nu^I \partial_\alpha \omega_\beta^I] \left[\frac{\eta_8}{2\sqrt{3}} + \frac{x\eta_0}{\sqrt{6}} \right] + \frac{z_W z_T^2}{z_A} \partial_\mu \phi_\nu^I \partial_\alpha \phi_\beta^I \left[-\frac{\eta_8}{\sqrt{3}} + \frac{x\eta_0}{\sqrt{6}} \right] \right\} \\ C = -\frac{N_c g^2 c_3}{8\pi^2 f_\pi} \end{array} \right. \quad (14)$$

in terms of ideal fields.

Actually, the γVP couplings relevant for our purpose can be derived from the following effective piece constructed from Eq. (14) above on the one hand, and from the $\gamma - V$ transitions of the non-anomalous Lagrangian [3] on the other hand (see Appendix A below) :

$$\left\{ \begin{array}{l} \mathcal{L}'_{AVP} = C' \epsilon^{\mu\nu\alpha\beta} F_{\mu\nu} \partial_\alpha A_\beta \quad , \quad C' = -\frac{N_c g e c_3}{12\pi^2 f_\pi} \\ F_{\mu\nu} = \left[\frac{1}{2}\pi^0 + \frac{\sqrt{3}}{2}\eta_8 + x\sqrt{\frac{3}{2}}\eta_0 \right] \partial_\mu \rho_\nu^I + \left[\frac{3}{2}\pi^0 + \frac{1}{2\sqrt{3}}\eta_8 + \frac{x}{\sqrt{6}}\eta_0 \right] \partial_\mu \omega_\nu^I + \left[\frac{1}{z_A} \sqrt{\frac{2}{3}}\eta_8 - \frac{x}{z_A \sqrt{3}}\eta_0 \right] \partial_\mu \phi_\nu^I \end{array} \right. \quad (15)$$

For the purpose of constructing the $X\pi^+\pi^-\gamma$ coupling at the chiral point, this piece fully replaces Eq. (14). It will be used together with the transition $\rho^I \rightarrow \pi^+\pi^-$ given by the non-anomalous Lagrangian⁴.

- The VPPP piece of relevance is :

$$\left\{ \begin{array}{l} \mathcal{L}_{VPPP} = -iD\epsilon^{\mu\nu\alpha\beta} \left\{ \rho_\mu^I \left[\frac{\sqrt{3}}{12}\partial_\nu\eta_8 + \frac{x\sqrt{6}}{12}\partial_\nu\eta_0 \right] + \frac{3}{4}\omega_\mu^I\partial_\nu\pi^0 \right\} \partial_\alpha\pi^- \partial_\beta\pi^+ \\ D = -\frac{N_c g}{4\pi^2 f_\pi^3} (c_1 - c_2 - c_3) \end{array} \right. \quad (16)$$

- The relevant APPP piece writes :

$$\left\{ \begin{array}{l} \mathcal{L}_{APPP} = -iE\epsilon^{\mu\nu\alpha\beta} A_\mu \left[\frac{1}{4}\partial_\nu\pi^0 + \frac{\sqrt{3}}{12}\partial_\nu\eta_8 + \frac{x\sqrt{6}}{12}\partial_\nu\eta_0 \right] \partial_\alpha\pi^- \partial_\beta\pi^+ \\ E = -\frac{N_c e}{3\pi^2 f_\pi^3} \left[1 - \frac{3}{4}(c_1 - c_2 + c_4) \right] \end{array} \right. \quad (17)$$

With these pieces at hand, one can compute the amplitudes at the chiral point. One first gets :

$$T(\pi^0 \rightarrow \pi^+\pi^-\gamma) = \frac{ieN_c}{12\pi^2 f_\pi^3} \left[1 + \frac{3}{4}(c_3 - c_4) \right] \quad (18)$$

which coincides with the amplitude expected from the WZW Lagrangian alone if $c_3 = c_4$. Assuming this condition, one can easily derive at the chiral point :

$$\left\{ \begin{array}{l} T(\eta_8 \rightarrow \pi^+\pi^-\gamma) = \frac{ieN_c}{12\pi^2 f_\pi^3} \frac{1}{\sqrt{3}} \quad , \quad T(\eta_0 \rightarrow \pi^+\pi^-\gamma) = \frac{ieN_c}{12\pi^2 f_\pi^3} \sqrt{\frac{2}{3}} x \end{array} \right. \quad (19)$$

which proves that the WZW usual (U(3)/SU(3) broken) amplitudes [14] at the chiral point are recovered. One may notice that the breaking matrices X_K and X_L play no role in the $X\pi^+\pi^-\gamma$ sector.

Therefore, assuming the conditions summarized in Eq. (13) leaves us with 2 more physics parameters unconstrained, compared with the previous version of our model : c_3 and $c_1 - c_2$. Using the information previously defined, the Extended Lagrangian we propose is :

$$\left\{ \begin{array}{l} \mathcal{L} = \mathcal{L}_A(z_A) + a\mathcal{L}_V(z_V) + \mathcal{L}_{YM}(z_T) + \\ \quad + \mathcal{L}_{VVP}(z_W) + \mathcal{L}_{AAP}(z_R = 1) + \mathcal{L}_{VPPP}(z_K = 1) + \mathcal{L}_{APPP}(z_L = 1) \\ c_4 = c_3 \\ z_W z_T^2 = 1 \end{array} \right. \quad (20)$$

⁴Anticipating on what is reminded in the next Section and relying on [3], this is justified by the fact that ideal vector fields and physical vector fields coincide at $s = 0$. Then, at $s = 0$, the couplings of the physical ω and ϕ mesons identically vanish, s being the square of the momentum carried by the vector meson.

where each SU(3) breaking parameter is exhibited with its value (when fixed). Out of these, the breaking parameters to be determined from data are z_A , z_V , z_T , x , keeping in mind that $z_A = [f_K/f_\pi]^2$ should always be satisfied⁵.

Such a price for the extension of the HLS model we propose looks acceptable, taking into account that we plan to describe all available anomalous processes beside $e^+e^- \rightarrow \pi^+\pi^-$ and $\tau^\pm \rightarrow \pi^\pm\pi^0\nu_\tau$ already accounted for within this model. This covers the $e^+e^- \rightarrow \pi^0\gamma$, $\eta\gamma$, $\pi^+\pi^-\pi^0$ cross sections and the box anomalous processes $\eta/\eta' \rightarrow \pi^+\pi^-\gamma$. A priori $e^+e^- \rightarrow \eta'\gamma$ data will fall into this extended scope when they will become available⁶.

4 Isospin Breaking And The (ρ , ω , ϕ) Mixing

We adopt here the (ρ , ω , ϕ) mixing developed in [3]. We only remind here a few properties for completeness and to simplify the notations. Let us define :

$$\begin{cases} \epsilon_1(s) = g_{\rho KK}^2(\Pi_+(s) - \Pi_0(s)) \\ \epsilon_2(s) = g_{\rho KK}^2(\Pi_+(s) + \Pi_0(s)) \\ \Pi_{\pi\pi}(s) = g_{\rho\pi\pi}^2\Pi'(s) \end{cases} \quad (21)$$

where $\Pi'(s)$ denotes the $\pi^+\pi^-$ amputated⁷ loop function, $\Pi_+(s)$ and $\Pi_0(s)$ the charged and neutral amputated kaon loops. The coupling constants occurring in Eqs. (21) fulfill $g_{\rho\pi\pi} = 2z_A g_{\rho KK} = ag/2$, in terms of the basic parameters of the model and of the SU(3) symmetry breaking parameter $z_A \equiv [f_K/f_\pi]^2$. These loop functions are analytic functions each real on the real s -axis below the corresponding threshold. At the limit of equal charged and neutral kaon masses, $\epsilon_1(s)$ vanishes ; on the other hand, both $\epsilon_1(s)$ and $\epsilon_2(s)$ have small magnitudes [3] in the whole s -region we are interested in (from the 2-pion threshold to the ϕ mass). Instead, $\Pi_{\pi\pi}(s)$ is basically the ρ self mass and is thus known to be significant in this s -region. The functions in Eqs. (21) are given by dispersion relations and contain each a polynomial in s chosen [3] of second degree and vanishing at the origin. These functions mainly serve to define three complex quantities⁸ :

$$\begin{pmatrix} \alpha(s) \\ \beta(s) \\ \gamma(s) \end{pmatrix} = \begin{pmatrix} \frac{\epsilon_1(s)}{\Pi_{\pi\pi}^\rho(s) - \epsilon_2(s)} \\ \frac{\mu\epsilon_1(s)}{(1 - z_V)m^2 + \Pi_{\pi\pi}(s) - \mu^2\epsilon_2(s)} \\ \frac{\mu\epsilon_2(s)}{(1 - z_V)m^2 + (1 - \mu^2)\epsilon_2(s)} \end{pmatrix} \quad (22)$$

⁵It could even be directly fixed to its experimental value $[f_K/f_\pi]^2 = 1.495 \pm 0.031$ without degrading the fits.

⁶A process like $e^+e^- \rightarrow \omega\pi^0$ is of this kind, however, one has first to carefully study the effects of scalars before any use of the corresponding data.

⁷*i.e.* with unit coupling constants.

⁸ The functions $\alpha(s)$, $\beta(s)$, $\gamma(s)$ defined here may be used all along this paper without exhibiting their functional (s) dependence. This notation makes easier reading the formulae given in Section 8 of [3] which are used in the present study. In order to avoid confusion, the fine structure constant is always denoted α_{em} .

where z_V is a parameter involved in the SU(3) symmetry breaking of the \mathcal{L}_V part of the non-anomalous HLS Lagrangian [4, 5, 3]. We have defined $\mu = z_V\sqrt{2}$, and $m^2 = ag^2f_\pi^2$ is the Higgs–Kibble ρ meson mass squared generated by the spontaneous breakdown of the HLS model. The complex quantities $\alpha(s)$, $\beta(s)$, $\gamma(s)$ are, in some sense, "angles" which describe the (ρ, ω, ϕ) mixing. At lowest (first) order in $\epsilon_1(s)$ and $\epsilon_2(s)$, the mixing scheme is given by :

$$\begin{pmatrix} \rho^I \\ \omega^I \\ \phi^I \end{pmatrix} = \begin{pmatrix} \rho^0 - \alpha\omega + \beta\phi \\ \omega + \alpha\rho^0 + \gamma\phi \\ \phi - \beta\rho^0 - \gamma\omega \end{pmatrix} \quad (23)$$

These relations exhibit the connexion between the "ideal" vector fields (carrying definite isospin properties), which are entries of the vector field matrix, and the "physical" fields (each a mixture of isospin 0 and 1 fields) which enter the physics processes. One may consider that $\alpha(s)$ is the $\rho - \omega$ (complex) mixing "angle" and that $\beta(s)$ and $\gamma(s)$ are, resp. the $\rho - \phi$ and $\omega - \phi$ mixing "angles". In our model, this mixing is s -dependent ; for instance, the $\omega - \phi$ mixing angle $\gamma(s)$ has not the same value at the ω mass and at the ϕ mass. Moreover, among these angles, $\gamma(s)$ is the single one to be practically real up to the ϕ mass region. Finally, as a consequence of $\alpha(0) = \beta(0) = \gamma(0) = 0$, physical (s -dependent) and ideal fields coincide at $s = 0$.

5 The ρ Propagators And The $\gamma - V$ Transition Amplitudes

The inverse propagators for the charged and neutral ρ can be written :

$$\begin{cases} D_{\rho^0}(s) = s - m^2 - \Pi_{\rho\rho}(s) \\ D_{\rho^\pm}(s) = s - m^2 - \delta m^2 - \Pi'_{\rho\rho}(s) \end{cases} \quad (24)$$

allowing for a possible $\rho^\pm - \rho^0$ mass difference. Neglecting the effects of mass differences between charged and neutral pseudoscalar mesons in the propagators, the same self-mass occurs, approximated by [3] :

$$\Pi_{\rho\rho}(s) = \Pi'_{\rho\rho}(s) = \Pi_{\pi\pi}(s) + \epsilon_2(s) \quad (25)$$

The notations defined in the previous Section allow one to express the $\gamma - V$ transition amplitudes in a more readable way than in [3] (see Section 8 there). The $\gamma - V$ transition amplitudes from photon to *physical* vector fields can be written as $eF_{V\gamma}(s)$ with :

$$F_{V\gamma}(s) = f_{V\gamma} - \Pi_{V\gamma}(s) \quad , \quad (26)$$

the constant term can be read off the $(V \cdot A)$ terms in the non-anomalous HLS Lagrangian and

the loop correction depends on the pion and kaon loops. The constant terms become :

$$\begin{cases} f_{\rho\gamma} = agf_\pi^2 \left[1 + \frac{1}{3}\alpha + \frac{\mu}{3}\beta \right] \\ f_{\omega\gamma} = agf_\pi^2 \left[\frac{1}{3} - \alpha + \frac{\mu}{3}\gamma \right] \\ f_{\phi\gamma} = agf_\pi^2 \left[-\frac{\mu}{3} + \beta + \frac{1}{3}\gamma \right] \end{cases} \quad (27)$$

and the s -dependent loop terms are [3] :

$$\begin{cases} \Pi_{\rho\gamma} = \left(1 - \frac{a}{2}\right) \frac{\Pi_{\pi\pi}^\gamma(s)}{g_{\rho\pi\pi}} + \left(z_A - \frac{a}{2} - b\right) \frac{\epsilon_1(s) + \epsilon_2(s)}{g_{\rho\pi\pi}} + b \frac{\epsilon_2(s) - \epsilon_1(s)}{g_{\rho\pi\pi}} \\ \Pi_{\omega\gamma} = -\left(1 - \frac{a}{2}\right) \alpha(s) \frac{\Pi_{\pi\pi}^\gamma(s)}{g_{\rho\pi\pi}} + \left(z_A - \frac{a}{2} - b\right) \frac{\epsilon_1(s) + \epsilon_2(s)}{g_{\rho\pi\pi}} - b \frac{\epsilon_2(s) - \epsilon_1(s)}{g_{\rho\pi\pi}} \\ \Pi_{\phi\gamma} = \left(1 - \frac{a}{2}\right) \beta(s) \frac{\Pi_{\pi\pi}^\gamma(s)}{g_{\rho\pi\pi}} - \left(z_A - \frac{a}{2} - b\right) \mu \frac{\epsilon_1(s) + \epsilon_2(s)}{g_{\rho\pi\pi}} + b\mu \frac{\epsilon_2(s) - \epsilon_1(s)}{g_{\rho\pi\pi}} \end{cases} \quad (28)$$

with $\mu = z_V \sqrt{2}$ and $b = a(z_V - 1)/6$. $\Pi_{\pi\pi}(s)$ (see Eq. (25)) and $\Pi_{\pi\pi}^\gamma(s)$ may carry different subtraction polynomials [3]. In the fit procedure described below, as in [3], their (second degree) subtraction polynomials are chosen independently and fit from data. Numerically, one finds no significant correlation among these 2 polynomials.

6 Combining Statistical and Systematic Uncertainties

For any of the data sets we use, there are reported statistical and systematic errors. One way to proceed is to add them in quadrature and define correspondingly a χ^2 to be minimized. If the errors are large enough, there is no real need to go beyond this simple treatment.

However, in samples where statistics is large, systematics should be handled a little bit more carefully. Systematic errors can be split up into two different kinds : uncorrelated and correlated uncertainties. It is quite traditional to combine uncorrelated systematic errors and statistical errors in quadrature and we follow this rule as, moreover, several data sets are provided with this combination already performed. When statistical errors are mentioned, this combination should be understood, unless explicitly stated.

It remains to handle the correlated systematic errors. As a first statement, one may interpret these as reflecting a global scale uncertainty which affects the data set considered. This was already done in our previous analysis [3]. Let us rephrase it with slightly more details, in order to explain clearly the method which underlies the present study.

6.1 Scale Uncertainties, A Reminder

The way statistical errors and scale uncertainties combine can be treated rigorously⁹. Let us assume one has a data set $m : \{m_i, i = 1, \dots, n\}$ and, correspondingly, a model $M : \{M_i, i =$

⁹We gratefully acknowledge P. Astier, LPNHE Paris 6/7, for several discussions on this subject.

$1, \dots, n\}$. Let us assume given its (symmetric) statistical error covariance matrix V which needs not be diagonal. Let us finally assume that a normalization scale uncertainty λ affects the data ; λ is supposed to have as most probable value 0 and standard deviation σ .

In this case, the conventional χ^2 is :

$$\chi^2 = [m - M - A\lambda]^T V^{-1} [m - M - A\lambda] + \frac{\lambda^2}{\sigma^2} \quad (29)$$

where A is traditionally the vector of the model values M and the other notations are obvious. For definiteness, in our study, we preferred using $A = -m$ in order to avoid having a covariance matrix depending on fit parameters¹⁰.

In this approach, λ is nothing but an additional constrained fit parameter. One can solve this equation at minimum χ^2 for λ using $d\chi^2/d\lambda = 0$ and substitute the expression for λ in Eq. (29). This leads to :

$$\chi^2 = [m - M]^T W^{-1}(\sigma^2) [m - M] \quad (30)$$

where :

$$W^{-1}(\sigma^2) = [V + \sigma^2 AA^T]^{-1} = V^{-1} - \frac{\sigma^2}{1 + \sigma^2(A^T V^{-1} A)} (V^{-1} A)(V^{-1} A)^T \quad (31)$$

which corresponds to Eqs (46) and (47) in [3]. If the expected value of λ were some $\lambda_0 \neq 0$, one has to replace in the second term of Eq.(29) λ^2 by $(\lambda - \lambda_0)^2$ and $m - M$ would become $m - M - A\lambda_0$ in Eq.(30). For practical use, if a scale uncertainty has been identified, data are generally corrected for this and then $\lambda_0 = 0$ is justified.

Eq. (30) illustrates that a correlated scale error is algebraically related with the model :

$$\lambda = \frac{A^T V^{-1} [m - M]}{A^T V^{-1} A + \frac{1}{\sigma^2}} \quad (32)$$

If the model depends linearly on parameters to be determined, the substitution has certainly to be performed in order to avoid the error covariance matrix of the (fit) parameters having a zero eigenvalue. If the dependence is non-linear, avoiding solving for λ only increases errors and produces (spurious) correlations.

Dealing with one (or several) data sample(s), the value of λ following from minimizing Eq. (29) can be confronted with the expected correlated systematic uncertainty. In practice, if the mean correlated systematic error has its correct value, one expects $|\lambda^{fit}|/\sigma$ small enough. In this case, having checked that $\lambda = 0$ is reasonable as expected, one can impose from start $\lambda \equiv 0$, *i.e.* minimize Eq. (30) ; one should then check that the fit probability and the parameter (hidden inside M) central values are nearly unchanged while the magnitude of their errors decreases.

In [3], we performed slightly differently : the scale uncertainty was considered as a random distribution $\delta\lambda$ of zero mean and of standard deviation σ which affects the measurements. One can check that this approach leads to the same conclusion which is summarized by Eq. (30). The present approach only clarifies that the final fit should be performed with $\lambda = 0$.

¹⁰ We checked with several of the fit configurations described below the difference between the two possible choices $A = M$ and $A = -m$. We did not observe differences beyond the 0.3σ level for the fit parameter values.

6.2 Checking And Dealing With A Missing Variance

However, as well known, identifying and estimating systematic uncertainties can be a delicate matter. Some source of systematics could have been missed or underestimated. When dealing with only one data set, this could well be quite transparent, as its effects could be absorbed by the other parameter values. However, while merging different data sets with different systematics, the pattern can be quite different and could result in poor fit probabilities. Therefore, it is useful to be in position of identifying a possible missing variance affecting some scale.

Let us assume the correct systematic variance of λ be $\sigma^2 + \eta^2$ instead of σ^2 . In this case the correct formula is Eq. (29) with $\sigma^2 \rightarrow \sigma^2 + \eta^2$. The question is now how to detect that a piece represented by η^2 could have been missed.

One can first check that :

$$\chi^2 = [m - M - A(\lambda_1 + \lambda_2)]^T V^{-1} [m - M - A(\lambda_1 + \lambda_2)] + \frac{\lambda_1^2}{\sigma^2} + \frac{\lambda_2^2}{\eta^2} \quad (33)$$

allows to recover the right result, provided one treats λ_1 and λ_2 as *independent* variables of zero mean and of respective variance σ^2 and η^2 . One can, moreover, check that :

$$\chi^2 = [m - M - A\lambda_2]^T W^{-1}(\sigma^2) [m - M - A\lambda_2] + \frac{\lambda_2^2}{\eta^2} \quad (34)$$

by solving, just as before, for only the identified systematics represented by the couple (λ_1, σ^2) . This equation gives us a handle to account for a missing (part) of the variance which could be revealed by using a large ensemble of data sets, each with its own systematics.

A way to check for a possible missing variance, is to compare a fitted λ_2 to the "identified" variance σ^2 . A tentative assumption for η^2 could be to state $\eta^2 \simeq \sigma^2$. Then, within a numerical fit procedure, one can check the magnitude of λ_2^{fit}/σ . If $|\lambda_2^{fit}|/\sigma$ is small enough ($\leq 1 \div 2$) a missing variance is certainly negligible compared with the identified one. Otherwise, the fit value of the scale indicates how much the data should be rescaled in order to match *all other data sets* and the model under test.

Of course, one thus makes an implicit statement : if the data sets which exhibit a significant missing variance represent a small minority, one may consider that this validates both a correction for missing variance and the model. If, instead, the data sets exhibiting a missing variance represent a majority, the model is certainly invalidated. Intermediate situations, if any, would be uncomfortable ; this might indicate some unaccounted for physics. Anyway, the set of data samples we consider does not face us with the latter configuration.

Finally, the χ^2 we shall deal with is a sum of partial χ^2 of the kind shown by Eq. (34). A first run of the fit procedure helps to identify which of the λ_2^α (α being the data set index) can be safely dropped out.

Concerning those which have still to be considered, one can keep the fit parameter as introduced. One should however keep in mind that this certainly enlarges the variance.

As a final remark, one should mention a rigorous way to lessen the variance. If some λ_2^α is considered significant, one should account for it, as the corresponding data set has certainly not been corrected for this source of uncertainties. However, a numerical minimization procedure like MINUIT provides an estimate of λ_2 – we name it λ_2^{fit} – and an estimate of its uncertainty

– we name it σ_{miss}^2 . – which can be accurately known running a code like MINOS. Then, the corrected (partial) χ^2 to be minimized can be rewritten :

$$\chi^2 = [m - M - \lambda_2^{fit} A]^T W^{-1} (\sigma^2 + \sigma_{miss}^2) [m - M - \lambda_2^{fit} A] \quad (35)$$

λ_2^{fit} can be estimated from Eq. (32) by changing σ^2 to $\eta^2 = \sigma_{miss}^2$. As one removes one free parameter, one almost certainly lessens the variance. This last expression depends on the other parameters under fit. A quite acceptable solution is instead to use the numerical minimizer output¹¹ for both λ_2^{fit} and σ_{miss}^2 , which makes the convergence easier.

7 The First Step In Modeling

In order to compare the pion form factor in e^+e^- annihilations and in τ decays, one has to account for isospin breaking effects which differ in both processes. The purpose of [3] was to show that the mixing between the ρ^0 , ω and ϕ mesons is responsible for most of the reported difference. We succeeded in determining the mixing model sketched above (mostly the "angles" $\alpha(s)$, $\beta(s)$, $\gamma(s)$) using the information provided by the anomalous decays of type $VP\gamma$ (and $P\gamma\gamma$) and the information carried by the isospin violating decays¹² $\omega/\phi \rightarrow \pi\pi$. In order to constrain more efficiently the parameter set, the partial widths $V \rightarrow e^+e^-$ ($V = \omega, \phi$) were also included. These pieces of information, as well as the ω/ϕ mass and width, were fixed at their accepted values [19]. We plan to examine the behavior of the Extended Model presented above while introducing more and more information to account for. For this purpose, we first focus on e^+e^- data, and as a first step on the $e^+e^- \rightarrow \pi^+\pi^-$ data mostly collected at Novosibirsk and already examined in [3] :

- the former data sets collected by the OLYA and CMD collaborations [20], and by DM1 at ACO [21] ; these were (and are still) together referred to as "old timelike data",
- the data sets more recently collected by the CMD-2 [22, 23, 24, 25] and SND [26] Collaborations, referred to globally as "new timelike data"
- all the partial widths for the decay processes of type $VP\gamma$, $P\gamma\gamma$, $\omega/\phi \rightarrow e^+e^-$ and $\phi \rightarrow \pi^+\pi^-$ at their updated recommended values [19]. These represent 17 pieces of information.

We gave up including the decay width $\eta' \rightarrow \rho\gamma$ (actually $\eta' \rightarrow \pi^+\pi^-\gamma$) as, in addition to the dominant triangle anomaly contribution, there is some (small) contamination by the box anomaly discussed already above. The decay modes $\eta/\eta' \rightarrow \pi^+\pi^-\gamma$ are revisited at the end of this study.

The systematic errors on the $e^+e^- \rightarrow \pi^+\pi^-$ cross sections just quoted are treated exactly as explained in Section 11.2 of [3], or as reminded above in Section 6, *i.e.* by summing in quadrature the statistical errors and the uncorrelated part of the systematic errors on the one hand, and, on the other hand, by accounting for the correlated systematic error through a global

¹¹In our case, the non-linear character of the model avoids having a singular parameter error covariance matrix while keeping the scale among the parameters to be fit.

¹²Actually, the $\omega \rightarrow \pi^+\pi^-$ mode has not to be included as it is already part of the $e^+e^- \rightarrow \pi^+\pi^-$ spectrum.

scale to be fit, at least for cross-check, as also explained in Section 6. The corresponding standard deviations to be introduced in the χ^2 are 0.4% for the "new timelike data" and 1.0% for the "old timelike data" [27]. The fitted scale values are expected negligible [3].

As our data samples contain all data used in order to get the recommended mass and width for the ω and ϕ mesons [19], we start here by leaving free the ω mass and width ; this could have easily been avoided at this step of our study by using [3] the world average values.

In addition, the present work uses the code delivered by F. Jegerlehner in order to calculate $\alpha_{em}(s)$ which can be downloaded from [28] ; this code, partly documented in [29], has been constructed in order to improve the estimates of the muon $g-2$ and of $\alpha_{em}(s)$ [30, 31, 32]. From there we get the photon (hadronic+leptonic) vacuum polarization (VP) building block, which is used by multiplying our model form factors, generically denoted $F(s)$, by the corresponding factor :

$$F(s) \implies \frac{1}{1 - \Delta\alpha_{em}(s)} F(s) \quad (36)$$

The package alphaQED.uu [28] also provides an estimate of the uncertainty on $\Delta\alpha_{em}(s)$.

In the extended model of this paper, the pion form factor has the same expression as in [3] :

$$F_\pi^e(s) = \left[\left(1 - \frac{a}{2}\right) - F_{\rho\gamma}^e(s) g_{\rho\pi\pi} \frac{1}{D_\rho(s)} - F_{\omega\gamma}^e(s) g_{\omega\pi\pi} \frac{1}{D_\omega(s)} - F_{\phi\gamma}^e(s) g_{\phi\pi\pi} \frac{1}{D_\phi(s)} \right] \quad (37)$$

where $D_\rho(s)$ is defined by the first Eq. (24) and by Eq. (25), while the other propagators are standard fixed width Breit–Wigner formulae. With our new notation set, the coupling constants simply write :

$$g_{\rho\pi\pi} = \frac{ag}{2} \quad , \quad g_{\omega\pi\pi} = -\frac{ag}{2}\alpha(s) \quad , \quad g_{\phi\pi\pi} = \frac{ag}{2}\beta(s) \quad (38)$$

On the other hand, the $VP\gamma$ coupling constants entering the corresponding partial widths in the extended model are essentially¹³ given by those in Eqs (E.1–E.4) of [3] *multiplied each by the new fit parameter c_3* . Instead, the couplings constants of type $P\gamma\gamma$ given by Eqs (E.5) in [3] are left unchanged as well as the leptonic decay widths of the vector mesons.

For definiteness, we have first performed the fit without including the photon VP. The most interesting results are reported in the first data column of Table 1. The results obtained when introducing the photon VP are given in the second data column in the same Table. One may already conclude that both descriptions provide a quite good account of the data sets considered. The first data column in Table 2 displays the fit value of the parameters having the most intuitive meaning while fitting with the photon VP. The values found for the fit scale factors exhibit a nice correspondence with the expectations reported in the experimental papers. One should also note that the fit value of the newly introduced fit parameter c_3 is statistically consistent with 1. This is in good correspondence with the fits presented in [3].

We do not discuss any further the intrinsic fit quality and fit parameter values as this case becomes interesting only compared to what happens when using additional data sets. We also do not show plots illustrating this fit quality : they are visually indistinguishable from Figure 2 in [3]. One may, however, remark that the probabilities are more favorable now ; this should

¹³Negligible correction terms are outlined in Section 13.

Data Set # (data + conditions)	Without VP	With Vacuum polarisation (VP)			
	NSK	NSK	$+(\pi^0/\eta)\gamma$	++ KLOE	+++ $\pi^0\pi^+\pi^-$
Decays	7.78/(17)	7.77/(17)	14.31/(9)	14.60/(9)	14.70/(9)
New Timelike (127+1)	114.83	114.09	114.12	127.15	127.75
Old Timelike (82+1)	54.80	53.86	50.84	49.32	49.32
KLOE (60+5)	–	–	–	108.39	108.21
$\pi^0\gamma$ (86)	–	–	61.38	62.07	65.66
$\eta\gamma$ (182)	–	–	128.55	129.73	135.20
χ^2/dof Probability	177.41/210 95.0 %	175.72/210 95.9 %	369.50/468 99.9%	491.27/528 87.2 %	637.90/653 65.6 %

Table 1: The first data column displays the partial χ^2 information while working with the largest set of partial widths and all available $e^+e^- \rightarrow \pi^+\pi^-$ data sets (except those of KLOE) and not taking into account the photon VP. The second data column displays the corresponding information while, instead, introducing the photon VP effects. In the third data column, the data concerning $e^+e^- \rightarrow \pi^0\gamma$ and $e^+e^- \rightarrow \eta\gamma$ are considered together with those on $e^+e^- \rightarrow \pi^+\pi^-$. In the following data column, the KLOE data are included and, correspondingly, the last data column gives the fit information while adding also the $e^+e^- \rightarrow \pi^0\pi^+\pi^-$ data (see text). Boldface numbers in the first data line display the number of (independent) partial widths which are included in the full fitted data sets.

be attributed marginally to using a different photon hadronic vacuum polarisation [28] and, especially, to having withdrawn the spacelike data [33, 34] from the fit procedure.

One may also note that the 17 accepted decay partial widths [19], which fully determine our symmetry breaking (SU(3)/U(3)/SU(2)) parameters, are all well accepted by the fit. At this stage, as in our previous study [3], only the $\rho^0 \rightarrow e^+e^-$ partial width significantly differs from its PDG value.

One should also note that introducing further cross section data sets has to be accompanied by the removal of all accepted partial widths [19] derived from – or highly influenced by – these additional data sets. It is the reason why the number of fit partial widths decreases from

17 to 9 as soon as the data on the $e^+e^- \rightarrow (\pi^0/\eta)\gamma$ annihilations are considered in addition to $e^+e^- \rightarrow \pi^+\pi^-$.

8 Including The $e^+e^- \rightarrow (\pi^0/\eta)\gamma$ Cross Section Data

8.1 Amplitudes and Cross Sections

Using the Lagrangians given in Appendices A and B, one can derive the transition amplitudes $\gamma^* \rightarrow P\gamma$. The matrix elements are :

$$\begin{cases} T(\gamma^* \rightarrow \pi^0\gamma) &= iY [g c_3 K_\pi(s) - (1 - c_3)L_\pi] \epsilon^{\mu\nu\alpha\beta} k_\mu \varepsilon_\nu(k) p_\alpha \varepsilon_\beta(p) \\ T(\gamma^* \rightarrow \eta_0\gamma) &= iY [g c_3 K_0(s) - (1 - c_3)L_0] \epsilon^{\mu\nu\alpha\beta} k_\mu \varepsilon_\nu(k) p_\alpha \varepsilon_\beta(p) \\ T(\gamma^* \rightarrow \eta_8\gamma) &= iY [g c_3 K_8(s) - (1 - c_3)L_8] \epsilon^{\mu\nu\alpha\beta} k_\mu \varepsilon_\nu(k) p_\alpha \varepsilon_\beta(p) \end{cases} \quad (39)$$

where $Y = -\alpha_{em} N_c / \pi f_\pi$, k is the incoming photon momentum ($k^2 = s$), p the outgoing photon momentum ($p^2 = 0$) and $N_c = 3$.

We have defined :

$$K_P(s) = \sum_{V_i=\rho^0,\omega,\phi} \frac{H_{V_i}^{Pj}(s) F_{V_i\gamma}(s)}{D_{V_i}(s)}, \quad P = \pi, \eta_0, \eta_8 \quad (40)$$

in terms of the $\gamma - V_i$ transition amplitudes $F_{V_i\gamma}$ (see Eq. (26)) and of the inverse propagators $D_{V_i}(s)$. $D_{\rho^0}(s)$ is given by Eq. (24), while the other inverse propagators are chosen of the form $s - m_V^2 + im_V \Gamma_V$ for the narrow ω and ϕ mesons. The functions $H_{V_i}^{Pj}$ which carry the dependence upon the isospin breaking angles $\alpha(s)$, $\beta(s)$ and $\gamma(s)$ are given by Eqs. (85) and refer to physical vector fields. We have also defined the constants :

$$L_\pi = \frac{1}{6}, \quad L_8 = \frac{1}{6\sqrt{3}} \frac{(5z_A - 2)}{3z_A}, \quad L_0 = \frac{x}{3\sqrt{6}} \frac{(5z_A + 1)}{3z_A} \quad (41)$$

which are terms deriving from the \mathcal{L}_{AAP} Lagrangian (see Eq. (86)). Defining the three following functions :

$$\begin{cases} R_\pi(s) = Y [g c_3 K_\pi(s) - (1 - c_3)L_\pi] \\ \begin{pmatrix} R_\eta(s) \\ R_{\eta'}(s) \end{pmatrix} = Y \begin{pmatrix} \cos \theta_P & -\sin \theta_P \\ \sin \theta_P & \cos \theta_P \end{pmatrix} \begin{pmatrix} g c_3 K_8(s) - (1 - c_3)L_8 \\ g c_3 K_0(s) - (1 - c_3)L_0 \end{pmatrix} \end{cases} \quad (42)$$

the $e^+e^- \rightarrow P\gamma$ cross sections are ($P = \pi^0, \eta, \eta'$) :

$$\sigma(s) = \frac{\alpha_{em}}{24} \left[\frac{s - m_P^2}{s} \right]^3 R_P^2(s) = \frac{3\alpha_{em}^3}{8\pi^2 f_\pi^2} \left[\frac{s - m_P^2}{s} \right]^3 |(g c_3 K_P(s) - (1 - c_3)L_P)|^2 \quad (43)$$

where m_P is the mass of the pseudoscalar meson produced in the annihilation process. K_P and L_P for $P = \eta, \eta'$ are trivially defined from $K_{0/8}$ and $L_{0/8}$ using Eqs. (42). θ_P , the

pseudoscalar mixing angle, is algebraically related with the breaking parameters x and z_A reminded above (see Eq. (E7) in [3]). Unfortunately, there is presently no available cross section data on the $e^+e^- \rightarrow \eta'\gamma$ channel. One can only use the $\phi \rightarrow \eta'\gamma$ branching fraction [19] as constraint ; however, one sees that the cross sections contain also definite constant terms (if fits confirm that $c_3 \neq 1$ is significant) and that these constant terms differ for η and η' . Therefore, the recommended branching fraction [19, 35] should be considered with some care, until a consistent analysis of the corresponding cross section becomes possible.

8.2 The Data Set Submitted To Fit

There are several data sets on the annihilation processes $e^+e^- \rightarrow \pi^0\gamma$ and $e^+e^- \rightarrow \eta\gamma$ available since 1999, all collected on VEPP-2M accelerator at Novosibirsk. In our analysis, we use all the data points up to $\sqrt{s} = 1.05$ GeV.

CMD-2 has recently published a data set on the final states $(\pi^0/\eta)\gamma$ (with $\pi^0/\eta \rightarrow \gamma\gamma$) from 600 to 1380 MeV [36] with 6 % systematic error. Previously, the same collaboration has published data [36] on the $\eta\gamma$ final state covering the same energy range and going through the mode $\eta \rightarrow 3\pi^0$; these data sets have 6.1% and 4.1% systematic errors, resp. below and above 950 MeV. We also use their former data set [37] on the $\eta\gamma$ final state, with $\eta \rightarrow \pi^+\pi^-\pi^0$, having a systematic error of 4.8%.

On the other hand, the SND Collaboration has also recently published [38] two different data sets for the $\eta\gamma$ final state with $\simeq 4.8$ % systematic errors, one with $\eta \rightarrow 3\pi^0$ from 600 to 1360 MeV, the other with $\eta \rightarrow \pi^+\pi^-\pi^0$ covering an energy range from 755 to 1055 MeV. A sample covering the energy range from 600 to 970 MeV for the $\pi^0 \rightarrow \gamma\gamma$ decay mode was also published [39]. Other data sets of 14 energy points between 985 and 1039 MeV were also published [40] with both final states $(\pi^0/\eta)\gamma$ (and $(\pi^0/\eta) \rightarrow 2\gamma$) and systematic errors of 2.5%.

Altogether, these two Collaborations provide 86 measurement points for the $e^+e^- \rightarrow \pi^0\gamma$ cross section and 182 for $e^+e^- \rightarrow \eta\gamma$ for $\sqrt{s} \leq 1.05$ GeV. These data are highly valuable in order to build up and thoroughly check our Extended Model in the anomalous sector.

In this second step, we consider altogether the three annihilation processes $e^+e^- \rightarrow \pi^+\pi^-$, $e^+e^- \rightarrow \pi^0\gamma$ and $e^+e^- \rightarrow \eta\gamma$. In order to constrain more our isospin symmetry breaking mechanism, we still include in the data set to be fit a part of the partial widths used in the previous Section and already used in [3]. Only 9 pieces of information are now independent of the present data : $\rho^\pm \rightarrow \pi^\pm\gamma$, $K^0 \rightarrow K^0\gamma$, $K^\pm \rightarrow K^\pm\gamma$, $\eta' \rightarrow \omega\gamma$, $\phi \rightarrow \eta'\gamma$, $\eta/\eta' \rightarrow \gamma\gamma$ and finally $\phi \rightarrow \pi^+\pi^-$ (in modulus and phase), which clearly carry information not statistically related with the cross sections considered.

Instead, as the recommended values [19] for $\omega/\phi \rightarrow e^+e^-$ are information highly influenced by the set of processes considered (and by the $e^+e^- \rightarrow \pi^+\pi^-\pi^0$ data considered later on), it is legitimate to let them free. This statement is *a fortiori* valid for the partial decay widths $\rho^0/\omega/\phi \rightarrow (\pi^0/\eta)\gamma$.

A last remark : the ω and ϕ masses and total widths are extracted from the data sets we consider. Therefore, it is certainly legitimate to let them vary. At the very end of our procedure, when the data on the $e^+e^- \rightarrow \pi^+\pi^-\pi^0$ annihilation process will have been considered, we will be in position to propose motivated averaged values for this information. Comparing with the results derived using the S-factor technics of the PDG [19] would become interesting.

Concerning our dealing with systematic errors for the newly introduced cross sections, we did not find numerically any need to split up correlated and uncorrelated systematic errors, which could have allowed increasing the fit parameter freedom. We therefore have simply added in quadrature systematic and statistical errors in order to compute the χ^2 to be minimized.

Finally, the $e^+e^- \rightarrow (\pi^0/\eta)\gamma$ cross sections submitted to fit have to be corrected for photon VP effects. This is done, as in the previous Section, by using the code provided by F. Jegerlehner [28].

8.3 Analysis of the Fit Results

The fit has been performed and the fit quality information is reported in the third data column of Table 1 and some fit parameter information is given in the second data column of Table 2.

In Table 1, one sees that the fit quality reached for the $e^+e^- \rightarrow \pi^0\gamma$ ($\chi^2/\text{points} \simeq 61/86$) as well as for $e^+e^- \rightarrow \eta\gamma$ ($\chi^2/\text{points} \simeq 129/182$) is very good.

Fig. 1 displays together the fit and data for the annihilation process $e^+e^- \rightarrow \pi^0\gamma$. The fit description is clearly quite good for these three data sets. Moreover, one should note that the fit values for the ω and ϕ peak locations are well centered compared to the data. The situation exhibited by Fig. 2 for the annihilation process $e^+e^- \rightarrow \eta\gamma$ is quite comparable. In the ω peak region, the large fluctuations in the experimental data prevent to be conclusive about the detailed lineshape returned by the fit, however, the ϕ mass region is nicely accounted for.

In Table 1, one should also note a significant increase of the χ^2 contribution of the decay modes : it practically doubles its value while the number of data is reduced by a half. A closer look at the results shows that the χ^2 contributions provided by 7 out of the 9 modes sums up to only 2.5, while $\chi^2(\phi \rightarrow \eta'\gamma) = 5.1$ and $\chi^2(\eta \rightarrow \gamma\gamma) = 6.9$, a 2.3σ and a 2.6σ effect respectively. One may not worry too much about the 2.3σ difference from the recommended value for $\text{Br}(\phi \rightarrow \eta'\gamma)$ for reasons already sketched ; however, a 2.6σ for $\text{Br}(\eta \rightarrow \gamma\gamma)$ could call for some comments.

When adding more and more spectra to be fit, the weight of isolated independent partial decay widths becomes generally less and less constraining. If needed, one may increase the weight of the decay mode of concern inside the full χ^2 . For instance, if instead of adding $\chi_{\eta \rightarrow \gamma\gamma}^2$ to the total χ^2 one adds $4 \times \chi_{\eta \rightarrow \gamma\gamma}^2$ or $8 \times \chi_{\eta \rightarrow \gamma\gamma}^2$ the distance to the recommended value becomes resp. 1.10σ or 0.72σ without a significant change to the "decay mode" contribution to the total χ^2 (it increases by 0.3 unit compared to the datum in Table 1). As this may look artificial, a more "natural" way would be to fix $z_A \equiv [f_K/f_\pi]^2 = 1.495 \pm 0.031$ at its (experimental) central value and use our model equations [5, 15, 3] :

$$\begin{cases} G_{\eta\gamma\gamma} = -\frac{\alpha_{em}}{\pi\sqrt{3}f_\pi} \left[\frac{5-2Z}{3} \cos\theta_P - \sqrt{2}\frac{5+Z}{3}x \sin\theta_P \right] , & \left(Z = \frac{1}{z_A} \right) \\ \tan\theta_P = \sqrt{2}\frac{Z-1}{2Z+1}x \end{cases} \quad (44)$$

to connect with the $\Gamma(P \rightarrow \gamma\gamma)$ datum [19] :

$$\Gamma(P \rightarrow \gamma\gamma) = \frac{m_P^3}{64\pi} |G_{P\gamma\gamma}|^2 , \quad (P = \pi^0, \eta, \eta') . \quad (45)$$

One could also derive the 1σ upper and lower bounds for x and z_A consistent with the f_K/f_π and $\Gamma(P \rightarrow \gamma\gamma)$ data and force the fit to stay within these limits¹⁴. Therefore, the problem encountered with $\Gamma(P \rightarrow \gamma\gamma)$ can easily be accommodated without any trouble.

On the other hand, it is useful to compare the fit parameter values derived in the present case with their analogs in the leftmost data column of Table 2. One first notes that the scale factors affecting the $e^+e^- \rightarrow \pi^+\pi^-$ data sets are left unchanged. The second remark concerns the physics parameters ; most of them vary well within the quoted 1σ uncertainties. The uncertainty for a is improved and its value is still significantly different from 2. The central value for x becomes closer to previous fit results using decay width data only [5, 14].

One should, however, note that c_3 becomes inconsistent with 1 by $\simeq 4.5\sigma$. This is clearly influenced by the anomalous branching fractions but also by the full cross section lineshapes of the anomalous annihilation processes we just considered. Forcing $c_3 = 1$ gives a fit quality $\chi^2(\phi \rightarrow \eta'\gamma) = 383.6/469$, almost as expected¹⁵.

It is worth noticing the ω and ϕ parameter values returned by the fit. At this step – before using $\pi^+\pi^-\pi^0$ data – we get $m_\omega = 782.45 \pm 0.05$ MeV and $\Gamma_\omega = 8.63 \pm 0.08$ MeV on the one hand, $m_\phi = 1019.25 \pm 0.02$ MeV and $\Gamma_\phi = 4.19 \pm 0.05$ MeV on the other hand. As will be seen later on, these values are modified while including 3–pion data.

9 Including The $e^+e^- \rightarrow \pi^+\pi^-$ Data From KLOE

The KLOE Collaboration, operating at the ϕ -factory DAΦNE, has recently published [13] the spectrum for the $e^+e^- \rightarrow \pi^+\pi^-$ form factor. Using the Initial State Radiation (ISR) mechanism, they produced a spectrum covering the region 0.60 – 0.97 GeV with very small statistical errors ($\simeq 0.5\%$). The systematic errors, also small, are dominant and have been thoroughly studied [41].

Several source of systematics are reported as (standard deviation) spectra representing fractions of the measured spectrum for $|F_\pi(s)|^2$. Their [13] Table 1 thus gives the uncertainty due to background subtraction ($\epsilon_1(s)$), their Table 2 displays the uncertainty due to acceptance corrections ($\epsilon_2(s)$) ; Table 3 and 4 respectively give the error due to detector resolution ($\epsilon_3(s)$) and the error due to the radiator function effects ($\epsilon_4(s)$). From their Table 5, one can derive by adding in quadrature the various source of systematics (other than the ones just listed) a global scale uncertainty ($\epsilon_0(s)$) of 0.76% for $|F_\pi(s)|^2$.

All these sources of uncertainty should be considered correlated except – maybe – for the error due to detector resolution (ϵ_3) which could have to be treated as uncorrelated [42]. This structure of systematic errors is clearly complicated and the question is how to deal with the error functions $\epsilon_\alpha(s)$ ($\alpha = 0, \dots, 4$) just defined.

The most appropriate way seems to follow the method presented in Section 6, *i.e.* each function $\epsilon_\alpha(s)$ is viewed as a gaussian random variable of zero mean and having s -dependent standard deviations (named $\eta_\alpha(s)$) given by the numbers in the Tables 1–5 of [13] for each Δs bin. More precisely, one may assume $\langle \epsilon_\alpha(s) \rangle = 0$, $\langle [\epsilon_\alpha(s)]^2 \rangle = [\eta_\alpha(s)]^2$ and $\langle \epsilon_\alpha(s_i)\epsilon_\beta(s_j) \rangle \simeq \delta_{\alpha\beta}\delta_{ij}$. This means that these five $\epsilon_\alpha(s)$ functions play as s -dependent scale

¹⁴Unless otherwise stated, the normal running conditions for our fits do not impose bounds to any parameter.

¹⁵The χ^2 difference with $\chi^2 = 369.5$ reported in Table 1 is found at 14.1 while one expects 19.4 ; this shows that the minimum is indeed close to parabolic.

Parameter	$e^+e^- \rightarrow \pi^+\pi^-$ (NSK Only)	$e^+e^- \rightarrow \pi^+\pi^-$ (NSK Only) $+ e^+e^- \rightarrow (\pi^0/\eta)\gamma$	$e^+e^- \rightarrow \pi^+\pi^-$ (NSK+ KLOE) $+ e^+e^- \rightarrow (\pi^0/\eta)\gamma$	All $e^+e^- \rightarrow \pi^+\pi^-$ $+ e^+e^- \rightarrow (\pi^0/\eta)\gamma$ $+ e^+e^- \rightarrow \pi^0\pi^+\pi^-$
Scale New Timelike	0.995 ± 0.004	0.996 ± 0.004	0.991 ± 0.004	0.991 ± 0.004
Scale Old Timelike	1.007 ± 0.009	1.007 ± 0.009	1.007 ± 0.009	1.007 ± 0.009
Scale KLOE 0	—	—	1.615 ± 0.816	1.621 ± 0.813
Scale KLOE 1	—	—	-0.041 ± 0.023	-0.041 ± 0.023
Scale KLOE 2	—	—	-0.070 ± 0.017	-0.070 ± 0.017
Scale KLOE 3	—	—	0.003 ± 0.006	0.003 ± 0.006
Scale KLOE 4	—	—	-0.011 ± 0.014	-0.011 ± 0.014
a	2.399 ± 0.022	2.356 ± 0.012	2.364 ± 0.011	2.365 ± 0.011
g	5.468 ± 0.021	5.574 ± 0.019	5.567 ± 0.013	5.568 ± 0.011
c_3	1.018 ± 0.017	0.943 ± 0.013	0.927 ± 0.013	0.930 ± 0.011
x	0.935 ± 0.014	0.904 ± 0.014	0.915 ± 0.014	0.914 ± 0.014
z_A	1.577 ± 0.020	1.467 ± 0.034	1.503 ± 0.020	1.496 ± 0.018
z_V	1.509 ± 0.020	1.425 ± 0.045	1.501 ± 0.030	1.503 ± 0.028
z_T	1.275 ± 0.053	1.301 ± 0.058	1.340 ± 0.059	1.332 ± 0.058

Table 2: Parameter values in fits performed including photon VP. The data subsamples included in the full data sample submitted to fit are indicated on top of the Table. The number of independent decay widths added to the data sample is 17 (first data column) or 9 (all other data columns). For the first 3 rescaling coefficients given in the Table, the corrections are the departure from 1, for all others, the rescaling are departures from 0.

uncertainties. Then a predicted value $|F_\pi(s_i)|^2$ should be associated with a datum m_i modified in the following way :

$$m_i \rightarrow m'_i = m_i \left[1 + \sum_{\alpha=0,1,2,3,4} \delta\lambda_\alpha(s_i) \right] \quad (46)$$

where each $\delta\lambda_\alpha(s_i)$ is one sampling of the corresponding random variable $\epsilon_\alpha(s)$ to be fitted.

Under these assumptions, the error covariance matrix writes in the usual way¹⁶ :

$$V_{ij} = \left[\sigma_i^2 + [\eta_3(s_i)|F_\pi(s_i)|^2]^2 \right] \delta_{ij} + \sum_{\alpha=0,1,2,4} \left[\eta_\alpha(s_i)|F_\pi(s_i)|^2 \right] \left[\eta_\alpha(s_j)|F_\pi(s_j)|^2 \right] \quad (47)$$

to be inverted numerically for χ^2 estimation. i, j are bin indices, while σ_i is the reported statistical error on m_i .

In practice, this turns out to compare the predicted function $|F_\pi(s)|^2$ following from a model to the modified data :

$$m'_i = m_i \left[1 + \sum_{\alpha=0,1,2,3,4} q_\alpha \eta_\alpha(s_i) \right] , \quad i = 1, \dots, n \quad (48)$$

where the five constants q_α are to be fit. Then, the partial χ^2 associated with KLOE data set is ($f_i \equiv |F_\pi(s_i)|^2$) :

$$\chi_{KLOE}^2 = \sum_{i,j} (m'_i - f_i)(m'_j - f_j) V_{ij}^{-1} + \sum_{\alpha=0, \dots, 4} q_\alpha^2 \quad (49)$$

In this way, one can check the consistency of q_α with respect to expectations as outlined in Section 6 and correct, if needed.

Finally, as the data under examination have not been corrected from photon VP effects, our fitting function is defined by Eqs. (36) and (37) given above.

We have submitted to fit the data set consisting of all the previously defined data subsets plus the KLOE data. The main results are reported in Table 1 (fourth data column) and Table 2 (third data column).

One first remarks from Table 1 that the fit probability is quite favorable (87 %). The χ^2 contribution from decays is as already reported in Section 8 and calls for the same comment (we have $\chi^2(\eta \rightarrow \gamma\gamma) = 2.7$ and $\chi^2(\phi \rightarrow \eta'\gamma) = 6.7$). Otherwise, the fit quality of the previously introduced (Novosibirsk) $\pi^+\pi^-$ timelike data is marginally degraded, while the description of the $(\pi^0/\eta)\gamma$ data is unchanged. The χ^2 contribution from the KLOE data set may look large but is still considered acceptable [42] ; this may reflect the unusual property of being highly dominated by systematic errors, always harder to estimate very precisely than statistical uncertainties. However, even if the χ_{KLOE}^2 is large, the global fit does not degrade significantly the fit quality of the other data sets and, moreover, the expected physics parameter values are not spoiled.

Some results referring to parameter values are reported in Table 2. One observes a change in the scale factor of the new timelike data which is shifted by 2σ from its expected value (0.4 %), while the scale factor associated with the old timelike data is unchanged ($\simeq 0.7\sigma$ from expectation). Out of the 5 scale parameters q_i specific to the KLOE data set, we find a global scale (q_0) correction at $\simeq (1.6 \pm 0.8)\sigma$ from the expected $\sigma = 0.76\%$; the parameter q_2 associated with the acceptance correction uncertainties is also significantly non-zero while all other corrections are small enough to be neglected.

Parameter values are slightly changed with using KLOE data. One should note the increased precision on g , the universal vector meson coupling. Finally, Fig. 3 shows superimposed the KLOE data, the fit function, together with the residuals. One clearly sees that the

¹⁶ This expression corresponds to having treated ϵ_3 uncorrelated. In this case, the sum on α in Eq. 49 does not extend to $\alpha = 3$. We tried both possibilities (uncorrelated and correlated) without getting significant differences.

description is reasonable. It should be noted however that the worst residuals are in the region covered by the ϵ_3 correction, *i.e.* the reported uncertainty on the detector resolution [13]. As far as we know, this is the first published fit to the available KLOE data.

10 Including $e^+e^- \rightarrow \pi^+\pi^-\pi^0$ Data

In contrast with the annihilation channels examined so far, the $e^+e^- \rightarrow \pi^+\pi^-\pi^0$ cross section involves the box anomaly sector presented in Section 2. It also involves the non-anomalous sector [3] and the triangle anomalies, as the $\pi^0\gamma$ and $\eta\gamma$ final states. This process allows to validate all sectors of the Extended HLS Lagrangian model, as defined at the beginning of this paper.

Without going into much details, one can list the Lagrangian pieces involved :

- The VVP piece (see Eq. (9)) expressed in terms of ideal vector fields has been already given expanded in [5]. This provides diagrams where the photon transforms to physical neutral vector fields with amplitudes given in Section 5. The transitions to $\rho\pi$ are given by :

$$\begin{cases} \mathcal{L}_{VVP} = C\epsilon^{\mu\nu\alpha\beta}F_{\mu\nu\alpha\beta} & , \quad C = -\frac{N_c g^2}{8\pi^2 f_\pi} c_3 \\ F_{\mu\nu\alpha\beta} = \partial_\mu \omega_\nu^I \left[\partial_\alpha \rho_\beta^I \pi^0 + \partial_\alpha \rho_\beta^+ \pi^- + \partial_\alpha \rho_\beta^- \pi^+ \right] + \dots \end{cases} \quad (50)$$

where the physical meson fields ω , ρ and ϕ appear when using Eqs. (23). The ρ^\pm particles decay with vertices as given in Eq. (79), while the neutral physical fields decay as follows :

$$\mathcal{L}_{VPP} = \frac{iag}{2} \rho_I^0 \cdot \pi^- \overleftrightarrow{\partial} \pi^+ = \frac{iag}{2} [\rho^0 - \alpha\omega + \beta\phi] \cdot \pi^- \overleftrightarrow{\partial} \pi^+ \quad (51)$$

This provides contributions symmetric in all $\rho\pi$ charge combinations. The argument of $\alpha(s)$, $\beta(s)$ and $\gamma(s)$ is always the incoming photon 4-momentum squared.

- The same VVP piece provides also a diagram without symmetric partners, where the $\gamma - \rho^0$ transition connects to $\omega\pi^0$ and the ω meson decays in accordance with Eq. (51). In this case the breaking function is $\alpha(s_{+-})$. The same piece provides also an unusual $\gamma - \rho^0$ term connecting with a $\rho^0 \rightarrow \pi^+\pi^-$ in the final state, with the same weight $\alpha(s_{+-})$.
- The APPP piece (see Eq. (9)) provides a single term $\gamma \rightarrow 3\pi$:

$$\mathcal{L}_{\gamma PPP} = ieD\epsilon^{\mu\nu\alpha\beta} A_\mu \partial_\nu \pi^0 \partial_\alpha \pi^+ \partial_\beta \pi^- & , \quad D = -\frac{N_C}{12\pi^2 f_\pi^3} \left[1 - \frac{3}{4}(c_1 - c_2 + c_3) \right] \quad (52)$$

to the amplitude, and depends on the newly introduced parameter $c_1 - c_2$.

- Finally, the VPPP piece contributes through the following piece of \mathcal{L}_{VPPP}

$$\mathcal{L}_{VPPP} = iE\epsilon^{\mu\nu\alpha\beta} \omega_\mu^I \partial_\nu \pi^0 \partial_\nu \pi^0 \partial_\alpha \pi^+ \partial_\beta \pi^- + \dots & , \quad E = -\frac{3N_c g}{16\pi^2 f_\pi} (c_1 - c_2 - c_3) \quad (53)$$

limiting oneself to the pion sector for the moment. Using Eqs. (23), one sees that each of the 3 physical neutral vector mesons may have a direct 3–pion coupling, however modulated by 1, $\alpha(s)$ and $\gamma(s)$ for resp. the ω , ρ^0 and ϕ mesons. s is still the incoming photon 4–momentum.

10.1 Matrix Element And Cross Section

The amplitude for the $\gamma^* \rightarrow \pi^+\pi^-\pi^0$ transition can be written :

$$T(\gamma^* \rightarrow \pi^+\pi^-\pi^0) = [T_{sym} + T_\rho] \epsilon^{\mu\nu\alpha\beta} \varepsilon_\mu(k) p_\nu p_\alpha^+ p_\beta^- \quad (54)$$

where $\varepsilon_\mu(k)$ ($k^2 = s$) is the (heavy) photon polarization vector. T_{sym} is the symmetric part of the amplitude (in terms of the $\rho\pi$ 'final' states), while T_ρ breaks this symmetry.

Using the $\gamma - V$ transition amplitudes given in Section 5, let us define¹⁷ :

$$\begin{cases} N_1(s) = \left[\frac{F_{\omega\gamma}(s)}{D_\omega(s)} + \alpha(s) \frac{F_{\rho\gamma}(s)}{D_{\rho^0}(s)} + \gamma(s) \frac{F_{\phi\gamma}(s)}{D_\phi(s)} \right] \\ N_2(s) = \left[\frac{1}{D_{\rho^0}(s_{+-})} + \frac{1}{D_{\rho^+}(s_{+0})} + \frac{1}{D_{\rho^-}(s_{-0})} \right] \\ N_3(s) = \alpha(s_{+-}) \left[\frac{1}{D_{\rho^0}(s_{+-})} - \frac{1}{D_\omega(s_{+-})} \right] \end{cases} \quad (55)$$

where the meaning of s_{+-} , s_{+0} and s_{-0} is obvious. Then, we have :

$$\begin{cases} T_{sym}(s) = \frac{ieN_c}{12\pi^2 f_\pi^3} \left[1 - \frac{3}{4}(c_1 - c_2 + c_3) + \frac{3}{2}m^2 g c_3 N_1(s) N_2(s) - \frac{9}{4}g(c_1 - c_2 - c_3) N_1(s) \right] \\ T_\rho(s) = \frac{ieN_c}{12\pi^2 f_\pi^3} \left[\frac{3}{2}m^2 g c_3 \right] \frac{F_{\rho\gamma}(s)}{D_{\rho^0}(s)} N_3(s) \end{cases} \quad (56)$$

The ρ propagators have already been defined by Eqs. (24) and (25). In order to study the three pion final state, we assume δm^2 (see Eq. (24)) to vanish ; the sensitivity to a non–vanishing δm^2 is certainly quite marginal as long as τ spectra are not considered.

As in Section 8, we approximate the ω and ϕ inverse propagators by :

$$\begin{cases} D_\omega(q^2) = q^2 - m_\omega^2 + im_\omega \Gamma_\omega \\ D_\phi(q^2) = q^2 - m_\phi^2 + im_\phi \Gamma_\phi \end{cases} \quad (57)$$

At the chiral point ($s_{+-} = s_{+0} = s_{-0} = s = 0$), T_ρ vanishes and one gets :

$$T_{sym}(0) = \frac{ieN_c}{12\pi^2 f_\pi^3} \quad (58)$$

¹⁷If the coupling of the charged ρ to a pion pair differs from the neutral one, g becoming $g + \delta g$, the last two terms in $N_2(s)$ should be affected by a factor of the form $1 + \delta g/g$. A test for a non–zero δg was performed in [3] using τ data and was not found significant.

from having required $c_3 = c_4$, and having assumed $[D_\omega(s=0)]^{-1} \equiv [D_\rho(s=0)]^{-1} = -m^2$. Therefore, one recovers the usual WZW term automatically at the chiral limit.

On the other hand, the differential cross section writes :

$$\frac{d^2\sigma(e^+e^- \rightarrow \pi^+\pi^-\pi^0)}{dx dy} = \frac{\alpha_{em}}{192\pi^2} s^2 G(x, y) |T_{sym} + T_\rho|^2 \quad (59)$$

when using the $(x$ and $y)$ parametrization proposed by [43] and summarized in Appendix C. One should note the abbreviated notation for the functions $G(x, y)$, $N_2(s)$ and $N_3(s)$ which are actually all functions of x , y and s .

10.2 Properties of the Matrix Element

The two pieces T_{sym} and T_ρ of our amplitude are given in Eqs. (56). It is easy to check that, in the limit of Isospin Symmetry conservation, the non-symmetric term T_ρ vanishes and that the symmetric part named T_{sym} reduces to only one term (with an intermediate ω).

As vector meson mixing occurs, the symmetric part T_{sym} clearly exhibits the 3 possible $\gamma - V$ transitions allowed by our Extended Lagrangian Model. The second term of T_{sym} is the more usual one, as it describes the sequence $e^+e^- \rightarrow V^0$ followed by $V^0 \rightarrow \pi^+\pi^-\pi^0$ through each of the $V^0\rho\pi$ possible couplings. One remarks that intermediate $V^0 = \rho^0$ or $V^0 = \phi$ are generated by Isospin Symmetry breaking.

The first term in T_{sym} is a non-resonant contribution $\gamma \rightarrow \pi^+\pi^-\pi^0$, specific of the HLS Lagrangian. It plays, for the 3-pions decay amplitude a role similar to the HLS a ($\simeq 2.4$) parameter for the $e^+e^- \rightarrow \pi\pi$ or $e^+e^- \rightarrow K\bar{K}$ amplitudes. The second term is the more usual one and should provide the dominant contribution.

The third term, instead, is the more problematic contact term [43] ; one sees that our model predicts that the 3 neutral vector mesons have a direct decay $V^0 \rightarrow \pi^+\pi^-\pi^0$ amplitude, with the ρ and ϕ contributions weighted by the mixing functions $\alpha(s)$ and $\gamma(s)$.

If one follows the educated guess expressed in [2] and thus fixes $c_3 = c_4 = c_1 - c_2 = 1$, the resonant contact term identically vanishes, while the non-resonant one survives with an intensity of -1/2, as supposed in a previous study on box anomalies [14]. As we do not expect large departures from the quoted guess, one can assert that the resonant contact term should indeed be very small. This is confirmed by the data and examined below.

Finally, one should note the dependence on $\alpha(s_{+-})$ of the non-symmetric part of the amplitude T_ρ . Actually, it is this special dependence which defines the non-symmetric amplitude. Other approaches generally consider only an ω term, while we also get a ρ term. Taking into account the large width of the ρ meson, one may guess that this term provides a tiny contribution.

10.3 The Data And The Fit Procedure

Here also a large number of data sets is available. The most significant are coming from CMD-2 and SND Collaborations running on the VEPP-2M machine at Novosibirsk.

CMD-2 has published several data sets with quoted uncertainties on the cross section merging statistical errors and uncorrelated systematic errors. The correlated systematic error, which

reflects the uncertainty on the global scale of the cross section, is given separately for each CMD-2 data set. The CMD-2 data sets to be considered are :

- The data set in [23] which covers the ω region and is claimed being affected by a global scale uncertainty of 1.3%,
- The data set given in [44] which covers the ϕ region, with a reported scale error of 4.6%,
- The ϕ region is also explored in [45], with a better reported scale uncertainty : 1.9%,
- The most recent CMD-2 data set is published in [46] and still covers the ϕ region with a favorable scale uncertainty (2.5%).

On the other hand, the SND Collaboration has published two spectra covering altogether the region from 0.440 to 1.38 GeV. We have considered all data points with $\sqrt{s} \leq 1.05$ GeV. These are :

- Below 980 MeV, the data set in [47],
- Above 980 MeV, the data set in [48]

SND preferred providing the statistical and systematic errors separately in their Tables. They claim that their detection efficiency and their integrated luminosity measurement merged together are actually a correlated systematic error. Therefore, all systematics, but these contributions, were added in quadrature to their statistical errors and we treated the rest as an uncertainty on the global scale of the cross section. This amounts to 3.4 % below 980 MeV [47] and we took 5% above [48].

For both CMD-2 and SND data, we treated the scale uncertainties as explained in Section 6. As in this case, we added penalty terms to the global χ^2 with the variance just quoted for each data set.

Besides these two groups of data samples, older data sets are worth considering :

- The former data sample collected by the ND Collaboration, with a reported systematic error of 10%, as given by the corresponding Table in the Physics Report by Dolinsky *et al.* [49].
- A small CMD data sample [50] – 5 measurements – covering the region in between the ω and ϕ peaks. The reported systematic error is 15 %.

The former covers the whole energy region between 0.75 and 1.38 GeV, but for our use, it was truncated at 1.05 GeV. All data points in this sample lay outside the ω and ϕ peak regions. Therefore, this allows us to constrain the most possible the non-resonant region which is well covered by SND, but more poorly by CMD-2. The data points being rather unprecise, there was no point in splitting up the systematic error into correlated and uncorrelated pieces ; we simply added them in quadrature with the reported statistical errors. We did alike for the CMD measurements [50].

Let us mention a DM1 data sample [49] which covers the energy region between 0.75 and 1.098 GeV. It could have been used, however, we are not sure of the systematics all along the spectrum. Therefore, we have preferred leaving it aside.

We still perform a global fit and, therefore, the data set submitted to fit always includes, together with specified 3 pion data subsets, all reported $\pi^+\pi^-$ Novosibirsk and KLOE data samples and all $e^+e^- \rightarrow (\pi^0/\eta)\gamma$ data sets.

From the point of view of a fit procedure, fitting 3–pion cross sections using the amplitude given in Eqs. (56) poses a problem of numerical analysis. Indeed, as clear from these equations, we have to integrate on the Kuraev–Siligadze [43] x and y variables at each step of the procedure a function which depends also on the parameters subject to minimization. This makes the computing time¹⁸ rather prohibitive.

However, having assumed that charged and neutral ρ have the same mass and the same coupling, the single parameter really influenced by 3–pion data is $c_1 - c_2$ (see Eq. (56)) ; all other parameters in functions to be integrated have already very precise fit values provided by the other data sets and are marginally influenced by the 3–pion data.

Therefore, the method we followed is to tabulate, in bins of $\Delta(\sqrt{s}) = 0.1$ MeV, the integrals over x and y of the $G(x, y)$ function alone and combined with the appropriate products of the N_i (see Eqs. (58)) and N_j^* functions *computed first from a minimization solution without 3–pion data*. Then one performs the global fit – including 3–pion data – using these functions. The fit result is then used to improve the integral calculations and restart a new minimization step. A priori, this procedure has to be repeated until some converge criterium is fulfilled.

We expected convergence in a very few steps. However, it so happens that there was no need to iterate the procedure, as the χ^2 was never changed by more than $\simeq 0.5$ unit, compared to some 'exact' computing method, where the integrals were computed at each minimization step. As the fit parameter values were not found to get significant corrections, we found justified to use this simplified method for performing our fits.

10.4 Exploratory Fits

Up to now, we have always used all available data sets for the various annihilation channels we have examined. The 3–pion data faces us with having to perform a choice between data sets which has to be motivated. It is the reason why some exploratory analysis of the 3–pion data sets has been worth performing.

We start by considering all CMD–2 [23, 44, 45, 46] and SND [47, 48] data sets in the less constraining pattern of our fit procedure ; namely, together with only the so–called old and new Timelike data sets collecting the standard $e^+e^- \rightarrow \pi^+\pi^-$ data sets. In this case, we have to use [3] also the full set of 17 accepted decay modes [19]. Indeed, doing this way :

- We lessen at most effects of $e^+e^- \rightarrow (\pi^0/\eta)\gamma$ on the value of c_3 , which plays some role in the 3–pion cross section,
- We avoid being sensitive to the KLOE data and their particular systematic errors.

¹⁸In order to analyze the behavior of each parameter or subset configuration, we need to run the code a large number of times. Without 3–pion fitting, such a run lasts about 2 minutes. Including the 3–pion samples, the fastest 'exact' method we found provides a waiting time of about an hour. The simplified method sketched below reduces the computing time to about 5 minutes per run.

Data Set ‡ (data + conditions)	Basic Fit	Global Fit with	Global Fit with ND+CMD ++		
	$\pi\pi + 3\pi$	ND+CMD	CMD2+SND	SND	CMD2
Decays	13.93/17	14.55/9	17.51/9	17.93/9	14.70/9
New Timelike (127+1)	116.29	127.05	129.53	130.07	127.76
Old Timelike (82+1)	49.89	49.35	49.99	50.08	49.32
KLOE (60+5)	—	108.45	105.11	102.69	108.21
$\pi^0\gamma$ (86)	—	62.06	72.04	82.61	65.66
$\eta\gamma$ (182)	—	129.84	133.64	131.81	135.20
CMD–2 [23] (13+1) *	28.31	—	27.14	—	25.05
CMD–2 [46] (47+1) *	58.24	—	53.89	—	52.48
CMD–2 [44] (16+1) *	17.84	—	17.78	—	15.76
CMD–2 [45] (13+1) *	21.76	—	20.82	—	13.86
ND+CMD [51] [50] (37)	31.47	25.82	23.78	23.58	25.94
SND [47] (49+1) *	47.94	—	67.22	63.55	—
SND [48] (33+1) *	54.62	—	77.75	55.59	—
g	5.641 ± 0.017	5.566 ± 0.010	5.599 ± 0.011	5.560 ± 0.010	5.568 ± 0.011
c_3	0.998 ± 0.017	0.927 ± 0.010	0.898 ± 0.010	0.895 ± 0.007	0.930 ± 0.011
$c_1 - c_2$	0.766 ± 0.056	1.168 ± 0.069	1.095 ± 0.039	1.012 ± 0.048	1.210 ± 0.043
corr ($c_3, c_1 - c_2$)	0.027	0.252	0.523	0.152	0.473
χ^2/dof	454.73/413	515.48/564	815.40/735	667.21/646	637.90/653
Probability	7.7 %	92.9 %	2.1 %	27.4 %	65.6 %

Table 3: Fit results using three–pion data sets within global fits. In the first line the number of decay widths is indicated in boldface. The so–called ‘conditions’ are the correlated scale uncertainties which are considered as data and fit. Comments are given inside the text. The partial χ^2 in lines flagged by * do not include the additional contribution of the scale factor. These are, nevertheless, counted inside the final χ^2 together with the number of conditions.

While comparing with other models and fits, one should keep in mind that, even if highly relaxed, our model is, nevertheless, sharply constrained. It is actually its lack of flexibility which imposes some good enough understanding of the experimental uncertainties and,

on the other hand, discloses the correlations between the various data sets imposed by the (common) underlying physics.

The fit pattern just described leads to the results reported in the first data column of Table 3. The fit qualities for the CMD–2 data sets given in [44, 46] are good ($\chi^2/\text{npoints} \simeq 1$) while the fit qualities of the data sets given in [23, 45] are worse ($\chi^2/\text{npoints} \simeq 1.5 \div 2$). The fit quality of the old ND [51] and CMD [50] data samples is also quite good ($\chi^2/\text{npoints} \simeq 1$ altogether). The low energy SND data set [47] returns a good fit quality ($\chi^2/\text{npoints} \simeq 1$), while the higher energy SND data set [48] is found worse ($\chi^2/\text{npoints} \simeq 1.5$). However, the global fit quality ($\chi^2/\text{npoints} \simeq 455/413$) corresponds to a 7.7% probability.

This relatively poor probability leads us to carefully examine the behavior of the CMD–2 and SND 3–pion data sets separately.

The next step relies on the following remark. All data sets – except for 3–pion data – allow to fix all parameters of our model, but $c_1 - c_2$. As can be seen from the third data column in Table 2, these are already known with an excellent accuracy, especially the parameters expected to be influenced by 3–pion data (g, c_3 for instance). Looking at Eqs. (56), one can easily see that the missing parameter $c_1 - c_2$ occurs in such a way that it is highly influenced by the invariant mass region outside both the ω and ϕ peaks. Therefore, one can guess that performing the global fit with the ND [51] and CMD [50] data samples only should allow a measurement of $c_1 - c_2$ with already a challenging accuracy. On the other hand, the Breit–Wigner mass and width for the ω and ϕ meson are accurately fit from the $(\pi^0/\eta)\gamma$ data.

Therefore, one can construct an accurate 3–pion cross section, valid for the whole energy range from threshold to above the ϕ mass, which feeds in the whole correlated physics information. This cross section can be used as a prediction to be compared to the data sets provided by the CMD–2 and SND Collaborations separately.

The global fit following this pattern has provided results shown in the second data column of Table 3. The global fit quality is well illustrated by the fit probability which reaches 93%. A closer look at the fit properties of the previous data sets shows that they are still optimally accounted for (compare this data column with the third data column in Table 2). The fit quality reached for the ND + CMD data set is also very good : $\chi^2/\text{npoints} \simeq 26/37$.

The accuracy reached for g and c_3 is unchanged, however this fit provides a value for $c_1 - c_2 \simeq 1.2$ with an accuracy of $\simeq 4\%$. Therefore, this allows us to define precisely the 3–pion cross section. This function is displayed in Figure 4 together with the CMD–2 and SND data superimposed in the ω region and in the ϕ region.

The left plots in Figure 4 show the case for CMD–2 data ; one can see that the data are already in good agreement with what can be inferred from ND+CMD data together with the physics of the other annihilation processes. The peak value and lineshape for the ω region are in accord with the prediction ; one may note, however, minor departures far on the wings. Concerning the ϕ region, the lineshape is in reasonable agreement with expectations, and one may infer that a fit will result in a good description.

Rightmost plots show the case for SND data ; at both the ω and ϕ peaks, one observes that both tops are $\simeq 10\%$ too large compared with the same expectations as before. However, a qualitative observation of the behavior in the ϕ region, allows one to infer that one should run into difficulties to account for both top and wings with only global (constant) rescalings.

This conclusion is substantiated with performing the global fit with all SND and CMD-2 data, as reported in the third data column in Table 3. In this case, the global fit probability reached is $\simeq 2\%$; the scale factors returned, 0.98 ± 0.03 for the low energy data sample [47] and 0.91 ± 0.04 for the higher energy one [48] are in good agreement with expectations. However, this poor fit probability, associated with poorer SND χ^2 's, indicates that the problem is not solved by means of constant rescaling factors.

Of course, this follows from having requested consistency of the 3-pion data sets, not only with each other, but also with all physically related annihilation processes. Indeed, one clearly understands that a common fit, using only the CMD-2 and SND 3-pion data, should certainly succeed with a solution intermediate between CMD-2 and SND data ; but this success would hide the consistency issue with the rest of related processes.

Therefore, the two global fits performed with merging SND and CMD-2 data tell us that there there is some inconsistency between them. Now, it remains to check separately SND +ND +CMD data, on the one hand and CMD2 +ND +CMD data, on the other hand, in order to make a motivated choice.

We have performed the global fit with all SND+ND+CMD data ; the results are reported in the fourth data column in Table 3. The global probability becomes more reasonable (27%) – from having removed CMD-2 data – and the fit rescaling factors are 0.96 ± 0.03 and 0.89 ± 0.04 for resp. the low and high energy regions. The fit quality exhibited for the low energy sample may look reasonable, however, the corresponding information for the higher energy data sample goes on looking poorer. This should reflect that the 10% scale correction, valid on the ϕ peak, is not appropriate on the wings.

The corresponding information from the global fit performed with all CMD-2+ND+CMD data is reported in the last data column of the same Table ; one gets a global fit probability of 66 %. This result, together with what is displayed in Figure 4, shows that ND+CMD data, on the one hand, and CMD-2 data, on the other hand, are quite consistent with each other.

Clearly, as the physics contents of the CMD-2 and SND data sets are the same, the issue just sketched cannot be attributed to our model. Because of Figure 4 and because of the respective probabilities, one has to choose among CMD-2 data and SND data, and the best motivated choice is the CMD-2 +ND +CMD solution. This also turns out to remark that Table 3 exhibits a poor consistency of SND data compared with ND +CMD. SND data are certainly useful, however not in the framework of a global fit which requires a good control of systematics in order to get reasonable consistency with all other physics process measurements.

10.5 The Solution With CMD-2, ND and CMD Data

Presently, the choice to remove the SND samples for 3-pions data considered in the global fit, seems the best motivated one. The main fit results are shown in the rightmost data column in Table 3. The fit is shown with data superimposed in Fig. 5. Top plots show a zoom on the peak regions, while the downmost plot focuses on the region outside the peaks. The fit is clearly satisfactory.

Let us summarize the other physics results of interest :

- The rescaling factors for all Novosibirsk and Frascati data reported in Table 2 are recovered with changes affecting the last digit, *i.e.* far inside the reported errors,

- the value for the HLS parameter $a = 2.365 \pm 0.105$ is also unchanged.
- The breaking parameters z_A , z_V and z_T were also left unchanged by the fit procedure, with unchanged uncertainties, compared with the third data column in Table 2.
- The scale factors found are 0.996 ± 0.012 for the data set in [23] (expected departure from 1 : 1.3%), 0.975 ± 0.020 for the data set in [46] quite in accord with the expected departure from 1 (2.5%). The other rescaling factors are resp. 0.953 ± 0.035 (data from [44] with expected departure from 1 of 4.6%) and 0.974 ± 0.016 (data from [45] with expected departure from 1 of 1.9%). Stated otherwise, the first 3 fit scales are 1σ at most from expectations, while the last scale is found at 1.25σ . This also indicates that there is no obvious signal of missing variance for the 3-pion CMD-2 data samples.

The fit quality for the ND data set in [51] and the old CMD data set [50] is quite satisfactory, The three CMD-2 data sets collected around the ϕ peak benefit from a $\chi^2/\text{npoints} \simeq 1$; instead, the χ^2 for the data set collected at the ω peak has a much poorer quality ($\chi^2/\text{npoints} = 25/13$). A closer look at the results shows that more than half of the χ^2 comes from 3 points on the wings¹⁹. However, as the global lineshape looks well reproduced at both peaks and in between them and also because of the good global fit quality, we consider the fit to the CMD-2, ND and CMD data as satisfactory.

Other fit information, reported in the last data column in Tables 1 and 2, allows estimating the effects of having included 3-pion data inside our fit data sample. Now, with the full information displayed, Table 1 clearly illustrates that the only noticeable changes (χ^2 increased by $\simeq 4$ units) concern the $\pi^0\gamma$ and $\eta\gamma$ data samples. Table 2 instead shows that there is no modification beyond the 1σ level.

11 A Few Numerical Results

With the fit presented just above, one ends up introducing data affecting the ω and ϕ mesons. Our global fit already provides interesting physics results which should not be affected by the forthcoming steps of our study.

11.1 ω and ϕ Masses And Widths

We have defined the ω and ϕ propagators as fixed width Breit–Wigner expressions (see Eqs. (57)). Our fits widely illustrate that there is no need to go beyond this approximation. As we account for both statistical and systematic errors, the uncertainties we quote fold in both kinds of errors and are thus directly comparable to RPP [19] information. Moreover, it should be noted that the RPP data on ω and ϕ masses and widths mostly relies on the data we have used.

¹⁹ The measurements located at $\simeq 0.76, \simeq 0.77$ and 0.80 GeV contribute resp. for 5, 4 and 6 units to the χ^2 .

Our final results are :

$$\left\{ \begin{array}{l} m_\omega = 782.42 \pm 0.05 \text{ MeV} \quad , \text{ RPP : } m_\omega = 782.65 \pm 0.12 \text{ MeV} \\ \Gamma_\omega = 8.700 \pm 0.084 \text{ MeV} \quad , \text{ RPP : } \Gamma_\omega = 8.49 \pm 0.08 \text{ MeV} \\ m_\phi = 1019.173 \pm 0.015 \text{ MeV} \quad , \text{ RPP : } m_\phi = 1019.455 \pm 0.020 \text{ MeV} \\ \Gamma_\phi = 4.259 \pm 0.036 \text{ MeV} \quad , \text{ RPP : } \Gamma_\phi = 4.26 \pm 0.04 \text{ MeV} \end{array} \right. \quad (60)$$

We thus find the ω mass 2σ below RPP average value and we get an uncertainty twice smaller. Γ_ω is found at 2.5σ from its recommended value [19], but in close agreement with the fit results of both the CMD-2 and SND Collaborations reported in the Review of Particle Properties [19].

The ϕ mass is instead found at 0.282 MeV from its recommended value [19] – about 20σ ! Interestingly, our extracted ϕ mass is also significantly smaller compared to the values extracted by CMD-2 and SND from the same data [19]. This might partly reflect the contributions of anomalous terms and the effect of vector meson mixing. Moreover, as parametrization of the propagator, we used a fixed width Breit–Wigner function, while CMD-2, for instance, used a varying width Breit–Wigner expression. Finally, Γ_ϕ is found in perfect agreement with the RPP for both the central value and its uncertainty.

One should note that our global fit is expected to :

- lessen the statistical error. Indeed, each parameter is constrained simultaneously by all data sets where it plays a role. This is, of course, true for the mass and width of the ω and ϕ mesons which sharply influence the $\pi^0\gamma$, $\eta\gamma$ and the $\pi^0\pi^+\pi^-$ final state descriptions ; moreover, the sharp drop observed in $e^+e^- \rightarrow \pi^+\pi^-$ is also influencing the ω meson parameters.
- perform the folding of systematic and statistical errors in accord with the whole knowledge of these uncertainties provided by the various experiments.

Therefore, the net expected result is an optimal folding in of all reported sources of errors, even when data are coming from different triggers and/or groups.

11.2 Contact Terms And Anomalous Lagrangians

A priori, the Extended HLS Model we use has two kinds of contact terms. One of the form γPPP describes the residual coupling of photons to pseudoscalar meson triplets, the other of the form $V PPP$ the direct coupling of a vector meson to a pseudoscalar meson triplet. The former is given (see Eq. (56)) by :

$$C_\gamma = 1 - \frac{3}{4}(c_1 - c_2 + c_3) = -0.61 \pm 0.10 \quad , \quad (61)$$

and the latter by the coefficient :

$$C_V = -\frac{9}{4}(c_1 - c_2 - c_3) = -0.63 \pm 0.31 \quad ; \quad (62)$$

this second coefficient is additionally modulated by $1, \alpha(s), \gamma(s)$ for resp. the ω, ρ, ϕ mesons when coupling to a pion triplet. The numerical values just given are derived from the information in Table 3 and include the effects of the covariance term $\langle \delta(c_1 - c_2) \delta c_3 \rangle$. These numbers are very close to the educated guess in [2] ($C_\gamma = -1/2$ and $C_V = 0$).

One can conclude that the contact term C_γ is certainly significant, while C_V has only a 2σ significance.

In view of these results, one is interested in seeing what happens to the global fit, if one fixes $c_3 = c_1 - c_2 = 1$ in the model. The result is shown in the second data column of Table 4. The subsamples not shown keep, roughly speaking, their usual χ^2 contributions. In this case, as could be expected, the fits to the $e^+e^- \rightarrow \pi^0\gamma$ and $e^+e^- \rightarrow \eta\gamma$ cross sections are significantly degraded and the global fit probability allows to reject this solution.

If one fixes $c_1 - c_2 = 1$ and leaves free c_3 (third data column in Table 4), the good description of $\pi^0\gamma$ and $\eta\gamma$ data sets is recovered as could be expected, but this is done at the expense of a worse description of $\pi^0\pi^+\pi^-$ data. The situation is similar if, instead, one fixes $c_3 = 1$ and let free $c_1 - c_2$.

One may conclude from the results collected in Table 4, that it is highly meaningful to let $c_1 - c_2$ and c_3 vary. This means that the violation of Vector Meson Dominance affects all sectors of the anomalous HLS Lagrangian [7, 2] ; this violation is only weaker in the Triangle sector than in the Box sector.

Global fit (χ^2 contributions)	$c_3, c_1 - c_2$ free	$c_3, c_1 - c_2$ fixed	$c_1 - c_2$ fixed	c_3 fixed
$\pi^0\gamma$ (86)	65.66	106.80	80.72	69.41
$\eta\gamma$ (182)	135.20	156.14	136.57	162.15
$\pi^0\pi^+\pi^-$ (130)	137.06	205.32	171.24	159.52
Probability	65.66 %	0.01 %	12.5%	12.7%

Table 4: Influence of the parameters c_3 and $c_1 - c_2$ on the fit results. Each entry displays the contribution to the total χ^2 of the quoted subsample. Last line provides the global fit probability. For the first column c_3 and $c_1 - c_2$ values are given in the last column of Table 3 ; the second column gives the best solution for $c_3 = c_1 - c_2 = 1$. In the third data column one has set $c_1 - c_2 = 1$ and the fit has returned $c_3 = 0.830 \pm 0.002$. In the fourth data column one has fixed $c_3 = 1$ and fit $c_1 - c_2 = 1.382 \pm 0.038$.

11.3 The Mixing 'Angles'

Most of the present data sets examined altogether are dominated by the ω and ϕ resonances. Using cross sections instead of only partial decay widths may produce changes in the mixing functions $\alpha(s)$, $\beta(s)$ and $\gamma(s)$ which, as noted before, can be interpreted as resp. the $\omega - \rho$, $\phi - \rho$ and $\omega - \phi$ mixing 'angles'. These are shown in resp. Figures 6, 7 and 8.

Compared to using only partial width decays together with $e^+e^- \rightarrow \pi^+\pi^-$ cross section data, one observes that the functions $\alpha(s)$ and $\beta(s)$ are unchanged (compare to Figure 7 in [3]). The function $\gamma(s)$, instead, gets significant changes. Figure 8 shows that the $\omega - \phi$ mixing angle becomes positive for $s > 0$, while it was negative when using partial width decays. However, the variation of $\gamma(s)$ remains significant between the ω and ϕ regions. The values which can be read off Figure 8 give $\gamma \simeq 2.75^\circ$ at the ω mass and $\gamma \simeq 3.84^\circ$ at the ϕ mass. As, now, one relies on the largest possible data set, this result should be considered as superseding the function $\gamma(s)$ in [3].

12 Validation Of The Model : The $\eta/\eta' \rightarrow \pi^+\pi^-\gamma$ Spectra

The amplitudes for $\eta/\eta' \rightarrow \pi^+\pi^-\gamma$ at the chiral point can be derived from the WZW Lagrangian [10, 11]. However, as there is no theoretical knowledge of their momentum dependence, modeling the behavior outside the chiral point is unavoidable. As shown by Eqs. (19), the Extended HLS Model allows to recover the chiral limit and the question is whether the predicted spectra and partial widths are in agreement with data. Such a study was already performed a few years ago [14] assuming, as inferred by [7, 2], that $c_1 - c_2 = c_3 = c_4 = 1$.

At the point where we are, all parameters of our Extended HLS Model have definite values and, thus, all vector meson and contact term contributions have no longer any free parameter. The question is now whether the spectra and the partial widths, which can be algebraically derived, fit the known physics information.

The most reliable physics information for these 2 decay modes is certainly their partial widths [19]. There exists two spectra giving the photon momentum distribution in the η rest frame [52, 53] ; however, the relevant information should be read off plots giving distributions for the measured spectrum and for the acceptance/efficiency function.

Understanding the dipion invariant mass spectrum in the $\eta' \rightarrow \pi^+\pi^-\gamma$ has been addressed several times, as most groups were claiming that the ρ mass peak was observed shifted. Most of these spectra were published only as figures [54, 55, 56, 57, 58] ; only Crystal Barrel provided the data points, feeding in the information concerning acceptance and efficiency corrections [59] ; some other spectra were only published as preprints or PhD theses. All these spectra were discussed in [14] and shown to exhibit very different qualities due to statistics [54] or, sometimes, to obvious biases [57], etc...

The issue was whether the ρ peak in the $\eta' \rightarrow \pi^+\pi^-\gamma$ spectrum is shifted. Crystal Barrel [59] clearly proved that the ρ peak location was indeed shifted by $\simeq 20$ MeV. The study in [14] later proved that this shift was actually the way found by fit procedures to account for a missing constant term which results in a distorsion of the ρ lineshape. This distorsion is produced by the contact term $\gamma\pi^+\pi^-\eta'$ which adds up with ρ meson contribution. Accounting for the contact term, [14] proved that the ρ peak in the η' spectrum is at the location expected

from $e^+e^- \rightarrow \pi^+\pi^-$ data. It is this question which is revisited within a framework where the condition $c_1 - c_2 = c_3 = c_4 = 1$ is violated and the vector meson mixing at work.

12.1 Amplitudes For The $\eta/\eta' \rightarrow \pi^+\pi^-\gamma$ Decays

Using the Lagrangian pieces given in Section 3, it is now easy to compute the transition amplitudes involved in the $\eta/\eta' \rightarrow \pi^+\pi^-\gamma$ decays. These can be derived from :

$$\begin{cases} T(\eta_8 \rightarrow \pi^+\pi^-\gamma) = A F_8(s) \epsilon^{\mu\nu\alpha\beta} \epsilon_\mu(\gamma) q_\nu p_\alpha^- p_\beta^+ \\ T(\eta_0 \rightarrow \pi^+\pi^-\gamma) = x\sqrt{2} A F_0(s) \epsilon^{\mu\nu\alpha\beta} \epsilon_\mu(\gamma) q_\nu p_\alpha^- p_\beta^+ \end{cases} \quad (63)$$

Having assumed $c_3 = c_4$, the octet and singlet functions write :

$$\begin{cases} F_8(s) = \left[1 - \frac{3c_3}{2} \left(1 + m^2 \sum_V \frac{c_V^8(s)}{D_V(s)} \right) \right] \\ F_0(s) = \left[1 - \frac{3c_3}{2} \left(1 + m^2 \sum_V \frac{c_V^0(s)}{D_V(s)} \right) \right] \\ A = -\frac{ieN_c}{12\pi^2 f_\pi^3} \frac{1}{\sqrt{3}} \end{cases} \quad (64)$$

where q is the photon 4-momentum and $s = (p^+ + p^-)^2$ is the dipion invariant mass. Neglecting terms of order greater than 1 in the mixing parameters α , β and γ , one has :

$$\begin{cases} \sum_V \frac{c_V^8(s)}{D_V(s)} = \left[1 + \frac{\alpha(s)}{3} - \frac{2\sqrt{2}}{3z_A} \beta(s) \right] \frac{1}{D_\rho(s)} - \frac{\alpha(s)}{3} \frac{1}{D_\omega(s)} + \frac{2\sqrt{2}}{3z_A} \frac{\beta(s)}{D_\phi(s)} \\ \sum_V \frac{c_V^0(s)}{D_V(s)} = \left[1 + \frac{\alpha(s)}{3} + \frac{\sqrt{2}}{3z_A} \beta(s) \right] \frac{1}{D_\rho(s)} - \frac{\alpha(s)}{3} \frac{1}{D_\omega(s)} - \frac{\sqrt{2}}{3z_A} \frac{\beta(s)}{D_\phi(s)} \end{cases} \quad (65)$$

which fulfill :

$$\sum_V \frac{c_V^0(s)}{D_V(s)} - \sum_V \frac{c_V^8(s)}{D_V(s)} = \frac{\sqrt{2}}{z_A} \beta \left[\frac{1}{D_\rho(s)} - \frac{1}{D_\phi(s)} \right] \quad (66)$$

The ϕ contributions in these expressions can be dropped out, because of the phase space cuts at $s = m_\eta^2$, or $s = m_{\eta'}^2$, much below the ϕ mass. Defining :

$$\begin{pmatrix} F_\eta(s) \\ F_{\eta'}(s) \end{pmatrix} = \begin{pmatrix} \cos \theta_P & -\sin \theta_P \\ \sin \theta_P & \cos \theta_P \end{pmatrix} \begin{pmatrix} F_8(s) \\ x\sqrt{2}F_0(s) \end{pmatrix} \quad (67)$$

the decay amplitudes for η and η' can be written :

$$T(\eta/\eta' \rightarrow \pi^+\pi^-\gamma) = A F_{\eta/\eta'}(s) \epsilon^{\mu\nu\alpha\beta} \epsilon_\mu(\gamma) q_\nu p_\alpha^- p_\beta^+ \quad (68)$$

and the decay partial width can be obtained by integrating :

$$\frac{d\Gamma(X \rightarrow \pi^+\pi^-\gamma)}{d\sqrt{s}} = \frac{1}{9} \frac{\alpha_{em}}{[2\pi f_\pi]^6} |F_X(s)|^2 q_\gamma^3 p_\pi^3 \quad , \quad X = \eta, \eta' \quad (69)$$

from the two-pion threshold to the η or η' mass. One has also defined $q_\gamma = (m_X^2 - s)/2m_X$ and $p_\pi = \sqrt{s - 4m_\pi^2}/2$.

12.2 Properties of the Amplitudes

The amplitudes just given have several interesting properties. As in the model developed in [14], one finds in Eqs (64) a vector meson amplitude which adds up with a non-resonant amplitude.

One might be surprised that these expressions do not depend on $c_1 - c_2$ as the decay amplitude for $e^+e^- \rightarrow \pi^0\pi^+\pi^-$. This is due to an unexpected conspiracy between the $VPPP$ and $APPP$ couplings (see Eqs. (16) and (17)) which both play a role in the transitions $\eta/\eta' \rightarrow \pi^+\pi^-\gamma$.

As for the amplitude for $e^+e^- \rightarrow \pi^+\pi^-$, the dipion invariant mass distribution exhibits an interference pattern between the ρ and ω meson contributions. However, all experimental data sets listed above indicate that this usual interference pattern should not be met, as there is no observed drop of the distributions around $\simeq 782$ MeV. The single difference between the $e^+e^- \rightarrow \pi^+\pi^-$ and $\eta' \rightarrow \pi^+\pi^-\gamma$ processes is that the term of order α is weighted by $1/3$ in the η' decay amplitude. It is thus interesting to see whether this different weighting alone allows to cancel out the (expected) drop in the dipion spectrum.

12.3 Comparison With Data

In Figure 9, one displays the dipion mass spectra in the $\eta' \rightarrow \pi^+\pi^-\gamma$ decay with, superimposed, the predictions coming out of the model fitting $e^+e^- \rightarrow \pi^+\pi^-$, $\pi^0\gamma$, $\eta\gamma$, $\pi^+\pi^-\pi^0$. We thus show the case for ARGUS data [56], for an experiment run at Serpukhov on the Lepton F facility [58] with relatively large statistics, and for Crystal Barrel [59], which is certainly the most precise η' spectrum. The last plot in Figure 9 is the spectrum of the photon momentum in the η rest frame for the $\eta \rightarrow \pi^+\pi^-\gamma$ decay [53], together with our prediction.

The agreement is satisfactory. One should note that some effect of the $\omega - \rho$ interference on the predicted lineshape can be detected but is not contradicted by the data. Actually, the data are binned and the curves shown are not averaged over the bin widths. One clearly sees that the peak location, as well as the global lineshapes are well predicted by our model. One may remark that the 20 MeV shift of the ρ peak confirmed by [59] is correctly reproduced. Therefore, having $c_3 \neq 1$ and vector meson mixing does not degrade the agreement already obtained in [14] with a much simpler model.

However, the quality of these data is not good enough to allow including the corresponding spectra into the global fit²⁰.

Other pieces of information are the partial widths for η and η' decays into this final state. The predicted values for these are :

$$\begin{cases} \Gamma(\eta' \rightarrow \pi^+\pi^-\gamma) = 53.11 \pm 1.47 \text{ keV} \\ \Gamma(\eta \rightarrow \pi^+\pi^-\gamma) = 55.82 \pm 0.83 \text{ eV} \end{cases} \quad (70)$$

²⁰Actually, the Crystal Barrel spectrum could be safely fit, except for a single point – at 812.5 MeV – which degrades severely the χ^2 without changing the parameter values at minimum. The Crystal Barrel spectrum is actually the merging of 4 spectra collected in $p\bar{p}$ annihilations at rest. Two of these (from $p\bar{p} \rightarrow \omega(\rightarrow \pi^0\gamma/\pi^0\pi^+\pi^-)\eta'$) exhibit this faulty point, for two others ($p\bar{p} \rightarrow \pi^0\pi^0\eta'$ and $p\bar{p} \rightarrow \pi^+\pi^-\eta'$) the corresponding measurement is located on the predicted curve. We have preferred avoiding to include a truncated spectrum inside our data set.

quite close to the corresponding recommended values [19] : 60 ± 5 keV and 60 ± 4 eV. The predictions are clearly quite accurate and provide support to the parameter values we derived from our global fit. This also indicates that we have exhausted our parameter freedom with the data set we already considered. Indeed, including these two pieces of information inside our global fit does not return results substantially different from the predicted values given just above. Therefore, the $\eta/\eta' \rightarrow \pi^+\pi^-\gamma$ decay modes represent a good test and better data on these decays would certainly be valuable in order to further constrain our model.

13 Decay Partial Widths Of Vector Mesons

Having allowed $c_3, c_1 - c_2 \neq 1$ in the HLS model [2], one allows other anomalous contributions than VVP to partial widths. Then, beside the diagrams represented by Fig. (10a), radiative decays of vector mesons get also contributions from diagrams as shown in Fig. (10b). These contributions are proportional to $1 - c_3$ and are generated by the AAP Lagrangian piece of our Extended Model. Correspondingly, the decay widths to 3 pions get their dominant contributions from diagrams generically represented by Fig. (10c), but also subleading $VPPP$ contributions proportional to $c_1 - c_2 - c_3$ from diagrams shown in Fig. (10d) and $APPP$ contributions (see Fig. (10e)) proportional to $1 - 3(c_1 - c_2 + c_3)/4$.

13.1 Radiative Decays Of Vector Mesons

As far as radiative decays are concerned, let us denote $g_{VP\gamma}$ the couplings generated by the VVP couplings and given in Appendix E of [3] where $c_3 = 1$ was assumed. In our Extended HLS Model, they become :

$$G_{VP\gamma} = g_{VP\gamma} c_3 \quad , \quad V = K^{*0}, K^{*\pm}, \rho^\pm \quad . \quad (71)$$

However, the couplings to ideal fields ($V_I = \rho_I, \omega_I, \phi_I$) yield additional corrections :

$$\left\{ \begin{array}{l} G_{V_I\pi^0\gamma} = g_{V_I\pi^0\gamma} c_3 - \frac{eD}{3} \frac{F_{V\gamma}(m_V^2)}{m_V^2} \quad , \quad D = -\frac{N_c e^2}{4\pi^2 f_\pi} (1 - c_3) \\ G_{V_I\eta^8\gamma} = g_{V_I\eta^8\gamma} c_3 - \frac{eD}{9\sqrt{3}} \left[\frac{5z_A - 2}{z_A} \right] \frac{F_{V\gamma}(m_V^2)}{m_V^2} \\ G_{V_I\eta^0\gamma} = g_{V_I\eta^0\gamma} c_3 - \frac{e x D}{9} \sqrt{\frac{2}{3}} \left[\frac{5z_A + 1}{z_A} \right] \frac{F_{V\gamma}(m_V^2)}{m_V^2} \end{array} \right. \quad (72)$$

The dominant VVP contributions are first order in g and are weighted by $c_3 \simeq 1$. The additional AAP contributions are of order e^2 and are additionally suppressed by $(1 - c_3)$. In the annihilation processes $e^+e^- \rightarrow \gamma P$, the AAP terms are subleading and are actually absorbed by the intermediate photon vacuum polarization in the e^+e^- annihilation amplitude. From a numerical point of view, these additional terms, all proportional to the $\gamma - V$ transition amplitudes $F_{V\gamma}(m_V^2)$, give a negligible contribution. These transitions amplitudes are given in Section 5. In order to compute the radiative decays of vector mesons, ideal field combinations have to be constructed [3], as reminded in Section 4. Also, pseudoscalar singlet and octet couplings have to be combined in order to derive the η and η' couplings [3]. The dependence upon the mixing 'angles' of vector mesons is hidden inside the $g_{VP\gamma}$ and $F_{V\gamma}$ functions.

13.2 Three Pion Decays of Vector Mesons

The coupling constants for three pion decays of neutral vector mesons can be derived in close correspondence with the $\gamma^* \rightarrow \pi^+\pi^-\pi^0$ amplitude constructed in Section 10. Let us define :

$$\begin{cases} M(x, y, s) = \frac{3}{2}m^2gc_3N_2(x, y, s) - \frac{9}{4}g(c_1 - c_2 - c_3) \\ C = 1 - \frac{3}{4}(c_1 - c_2 + c_3) \\ E = -\frac{N_c}{12\pi^2f_\pi^3} \end{cases} \quad (73)$$

fully displaying the dependence upon the Kuraev–Siligadze [43] variables. The function $N_2(x, y, s)$ has been defined in Section 10 and $m^2 = ag^2f_\pi^2$. Then, the amplitudes for $V \rightarrow \pi^+\pi^-\pi^0$ are, at leading order in the symmetry breaking parameters :

$$\begin{cases} A_\omega(x, y) = E \left[M(x, y, m_\omega^2) + e^2C \frac{F_{\omega\gamma}(m_\omega^2)}{m_\omega^2} \right] \\ A_\phi(x, y) = E \left[\gamma(m_\phi^2)M(x, y, m_\phi^2) + e^2C \frac{F_{\phi\gamma}(m_\phi^2)}{m_\phi^2} \right] \\ A_\rho(x, y) = E \left[\alpha(m_\rho^2)M(x, y, m_\rho^2) + \frac{3}{2}m^2gc_3N_3(x, y, m_\rho^2) + e^2C \frac{F_{\rho\gamma}(m_\rho^2)}{m_\rho^2} \right] \end{cases} \quad (74)$$

where $N_3(x, y, s)$ has also been defined in Section 10 and hides a dependence upon $\alpha(s_{+-})$ (s_{+-} being the $\pi^+\pi^-$ squared invariant mass of the decay products). One may observe that the dominant terms for ρ and ϕ are generated by vector meson mixing and that there is a specific term in the ρ amplitude compared to those for ω and ϕ . One should also note that the $APPP$ coupling generates a subleading term (of order e^2) which exists even if there were no vector meson mixing. The present model is more complicated than the one developed by [43] because of these $APPP$ terms and of the vector meson mixing.

Finally, in terms of the amplitudes given in Eqs. (74), the 3–pion partial widths are given by [43] :

$$\Gamma(V \rightarrow \pi\pi\pi) = \frac{m_V^7}{768\pi^3} \int \int dx dy G(x, y) |A_V(x, y)|^2 \quad (75)$$

where the function $G(x, y)$ [43] has been reminded in Appendix C.

13.3 Effects Of A $\mathcal{O}(p^4)$ Lagrangian Piece

In [60], Harada and Yamawaki have studied the Wilsonian matching of the HLS model with QCD. For this purpose they have identified 35 $\mathcal{O}(p^4)$ Lagrangian pieces of the HLS Lagrangian which are provided explicitly in [2]. Among these, one is of special interest for our purpose, the so–called z_3 term which is of concern for the $\gamma - V$ and $W - V$ transitions. Discarding

effects of SU(3) symmetry breaking, the additional Lagrangian piece writes :

$$\left\{ \begin{array}{l} \mathcal{L}_4 = \mathcal{L}_4^\gamma + \mathcal{L}_4^{W^+} + \mathcal{L}_4^{W^-} \\ \mathcal{L}_4^\gamma = 2z_3 g e \partial_\mu A_\nu \left[(\partial_\mu \rho_\nu^I - \partial_\nu \rho_\mu^I) + \frac{1}{3} (\partial_\mu \omega_\nu^I - \partial_\nu \omega_\mu^I) - \frac{\sqrt{2}}{3} (\partial_\mu \phi_\nu^I - \partial_\nu \phi_\mu^I) \right] + \dots \\ \mathcal{L}_4^{W^+} = z_3 g g_2 V_{ud} \partial_\mu W_\nu^+ (\partial_\mu \rho_\nu^- - \partial_\nu \rho_\mu^-) + \dots \\ \mathcal{L}_4^{W^-} = z_3 g g_2 \bar{V}_{ud} \partial_\mu W_\nu^- (\partial_\mu \rho_\nu^+ - \partial_\nu \rho_\mu^+) + \dots \end{array} \right. \quad (76)$$

using notations already defined in [3] and reminded above. This turns out to modify in exactly the same way the transition amplitudes for $\gamma - V$ and $W - V$ by adding a s -dependent term to the constant part of the couplings. More precisely, one gets (see Eqs. (30) in [3] for τ decays and Section 5 above for e^+e^- annihilations) :

$$\left\{ \begin{array}{l} f_\rho^\tau \implies f_\rho^\tau \left(1 - \frac{z_3}{a f_\pi^2} s \right) \\ f_{V\gamma} \implies f_{V\gamma} \left(1 - \frac{z_3}{a f_\pi^2} s \right) \end{array} \right. \quad (77)$$

where z_3 can be related with the Low Energy Constant (LEC) L_9 of the Chiral Perturbation Theory. When on mass shell, the additional factor is simply $(1 - g^2 z_3)$ and can be guessed [2] of the order 1.10. Indeed, even if z_3 is expected small, the g^2 term produces an important enhancement factor.

However, in processes like e^+e^- annihilations or τ decay, f_ρ^τ or $f_{V\gamma}$ always come in combination with the loop dressing functions [3] $\Pi_W(s)$ or $\Pi_{V\gamma}(s)$ which contain subtraction polynomials to be fitted. Therefore, the z_3 contribution comes in entangled with the first degree term of the subtraction polynomial and cannot be singled out. As a consequence, the fit value for g may absorb effects of the z_3 correction and may produce too low values by as much as 10% for the amplitudes [2].

In the e^+e^- annihilation channels considered in the present work, our fit procedure is sensitive to the product $F_{V\gamma} \times g$ for each resonance rather than to the $F_{V\gamma}$'s and g separately²¹. The fit quality we have reached allows us to consider that these products are well understood. Therefore, all pieces of information relying on these products can be considered reliable. This covers all products of widths like $\Gamma(V \rightarrow P\gamma)\Gamma(V \rightarrow e^+e^-)$ or $\Gamma(V \rightarrow \pi^+\pi^-\pi^0)\Gamma(V \rightarrow e^+e^-)$. Ratios of widths performed from the $\Gamma(V \rightarrow P\gamma)$'s and $\Gamma(V \rightarrow \pi^+\pi^-\pi^0)$'s are also free from the disease mentioned above and can be considered as secure. It is the reason why we will not go beyond these products and ratios until a satisfactory solution to the issue just mentioned is found.

Actually, some possibilities exist to solve this ambiguity, at least in principle. Indeed, processes like $e^+e^- \rightarrow \mu^+\mu^-$ are sensitive to the $[F_{V\gamma}]^2$'s and could be used. Some scarce

²¹In our full data set, only the radiative decays of the K^{*0} , $K^{*\pm}$, ρ^\pm do not belong to this category, but are not sufficient to modify the picture.

(accurate) data (3 measurement points) at the ϕ mass are reported [62] but, unfortunately, nothing with the required accuracy is reported around the ω mass. Another possibility could be to examine channels like $e^+e^- \rightarrow \omega(\rightarrow \pi^0\gamma)\pi^0$ which are rather sensitive to some of the $F_{V\gamma} \times g^2$'s. Finally, one could also fix the leptonic widths as coming from the fits of the Particle Data Group [19], which basically corresponds to our results published in [3]. This last solution, even if legitimate, is not completely satisfactory.

It should be stressed that the effect mentioned is actually common to any parametrization of e^+e^- and τ data and is by no means specific to the HLS Model (see, for instance, the discussion in [43]). On the other hand, reporting on products and ratios is the standard way experimental groups proceed with the kind of data we are dealing with and we may compare to these.

Data	Our Fit	PDG 2008
$\Gamma'(\rho^0 \rightarrow \pi\pi) \times 10^5$	4.72 ± 0.02	$4.876 \pm 0.023 \pm 0.064$
$\Gamma'(\omega \rightarrow \pi\pi) \times 10^6$	1.146 ± 0.057	$1.225 \pm 0.058 \pm 0.041$
$\Gamma'(\rho^0 \rightarrow \pi^0\gamma) \times 10^8$	1.875 ± 0.026	2.8 ± 0.4
$\Gamma'(\omega \rightarrow \pi^0\gamma) \times 10^6$	6.80 ± 0.13	6.39 ± 0.15 **
$\Gamma'(\phi \rightarrow \pi^0\gamma) \times 10^7$	4.29 ± 0.11	3.75 ± 0.18
$\Gamma'(\rho^0 \rightarrow \eta\gamma) \times 10^8$	1.05 ± 0.02	1.42 ± 0.10
$\Gamma'(\omega \rightarrow \eta\gamma) \times 10^8$	4.50 ± 0.10	3.31 ± 0.28 **
$\Gamma'(\phi \rightarrow \eta\gamma) \times 10^6$	4.19 ± 0.06	3.87 ± 0.07 **
$\Gamma'(\rho^0 \rightarrow \pi\pi\pi) \times 10^{10}$	9.03 ± 0.76	$45.8_{-16.4}^{+24.6} \pm 15.6$ **
$\Gamma'(\omega \rightarrow \pi\pi\pi) \times 10^5$	6.20 ± 0.13	6.39 ± 0.10
$\Gamma'(\phi \rightarrow \pi\pi\pi) \times 10^5$	4.38 ± 0.12	4.53 ± 0.10

Table 5: Results for $\Gamma'(V \rightarrow f) \equiv \Gamma(V \rightarrow e^+e^-)\Gamma(V \rightarrow f)/\Gamma_{tot}^2$ for each V vector meson and each final state f . The most significant results are flagged by **.

13.4 Results For Partial Widths

In Table 5, we give our fit results for :

$$\Gamma'(V \rightarrow f) \equiv \Gamma(V \rightarrow e^+e^-)\Gamma(V \rightarrow f)/\Gamma_{tot}^2$$

and provide the measurements collected in the RPP [19]. The results on which we report have been derived from a fit to all e^+e^- annihilation data, except for KLOE data [12], by fixing the scale corrections to zero in accordance with Section 6.

One thus notes that, for most of the reported products, one gets results in accordance with what is extracted from the same data. One should remember that the errors we quote fold in systematic and statistical errors and can be compared to the averages performed by the Particle Data Group.

Concerning $\rho^0 \rightarrow \pi\pi\pi$, our result, mostly determined by CMD-2 data, is in agreement with the SND result, but with a much lower central value and a much better accuracy. Significant differences mostly concerning $\omega/\phi \rightarrow \eta\gamma$ can be read off Table 5. They correspond to performing a simultaneous fit of all the involved data which happens to be of very high quality as shown in Section 10 above. Finally, as a general statement, our uncertainties reported in Table 5 are either of magnitude comparable to the existing information or of much better accuracy.

Data	Our Fit	PDG 2008
$\Gamma(\rho^0 \rightarrow \pi\pi)/\Gamma(\rho^0 \rightarrow \pi\pi\pi)$	$(5.26 \pm 0.45) 10^4$	> 100
$\Gamma(\omega \rightarrow \pi\pi)/\Gamma(\omega \rightarrow \pi\pi\pi)$	$(18.5 \pm 1.0) 10^{-3}$	$(17.2 \pm 1.4) 10^{-3}$
$\Gamma(\rho^0 \rightarrow \pi\gamma)/\Gamma(\rho^0 \rightarrow \pi\pi\pi)$	20.91 ± 1.60	[5.94 ± 3.36]**
$\Gamma(\omega \rightarrow \pi\gamma)/\Gamma(\omega \rightarrow \pi\pi\pi)$	0.110 ± 0.003	0.0999 ± 0.0026 **
$\Gamma(\phi \rightarrow \pi\gamma)/\Gamma(\phi \rightarrow \pi\pi\pi)$	$(9.80 \pm 0.29) 10^{-3}$	(8.3 ± 0.6) 10⁻³
$\Gamma(\rho^0 \rightarrow \pi\pi)/\Gamma(\rho^0 \rightarrow \pi^0\gamma)$	$(2.52 \pm 0.03) 10^3$	(1.74 ± 0.27) 10³
$\Gamma(\omega \rightarrow \pi\pi)/\Gamma(\omega \rightarrow \pi^0\gamma)$	0.169 ± 0.009	0.20 ± 0.04
$\Gamma(\rho^0 \rightarrow \eta\gamma)/\Gamma(\rho^0 \rightarrow \pi^0\gamma)$	0.561 ± 0.008	(0.50 ± 0.08)
$\Gamma(\omega \rightarrow \eta\gamma)/\Gamma(\omega \rightarrow \pi^0\gamma)$	$(6.62 \pm 0.17) 10^{-3}$	$(9.8 \pm 2.4) 10^{-3}$ **
$\Gamma(\phi \rightarrow \eta\gamma)/\Gamma(\phi \rightarrow \pi^0\gamma)$	9.77 ± 0.20	$10.9 \pm 0.3 \pm 0.7$

Table 6: Ratios of Widths. In the second data column, number written in plain style are directly extracted from the Review of Particle Properties, the boldface ones are derived from making the ratios of the accepted branching ratios [19]. The most significant results are flagged by **.

As our fit procedure is global, it also allows to relate different decay modes of the same vector meson. These are provided in Table 6 with information extracted from the most recent RPP [19]. Taking into account the fit quality of the corresponding cross sections, the difference with RPP expectations should be considered significant.

One should first remark the ratio $\Gamma(\rho^0 \rightarrow \pi\gamma)/\Gamma(\rho^0 \rightarrow \pi\pi\pi)$ which is found $\simeq 3.5$ larger than expected from the ratio of branching ratios as given in [19], with a significance of $\simeq 4\sigma$. Less impressive but, nevertheless, significant is the corresponding ratio for the ω meson.

More interesting, however, is the ratio $\Gamma(\omega \rightarrow \eta\gamma)/\Gamma(\omega \rightarrow \pi^0\gamma)$ which is found much more precise than (old) existing measurements and benefits from being derived by means of a

simultaneous fit to all recent relevant data sets.

14 Conclusion

The model developed in [3] succeeded in accounting for 17 decay modes of vector mesons and in providing a good simultaneous description of the $e^+e^- \rightarrow \pi^+\pi^-$ cross section and of the dipion spectrum in τ decay. The present paper has shown that it can be easily extended in order to provide also a successful description of the $e^+e^- \rightarrow \pi^0\gamma$, $e^+e^- \rightarrow \eta\gamma$ and $e^+e^- \rightarrow \pi^0\pi^+\pi^-$ cross sections and account precisely for the properties of the $\eta/\eta' \rightarrow \pi^+\pi^-\gamma$ decays. Its application to $e^+e^- \rightarrow K\bar{K}$ decay mode is postponed to another study, because of the problem stated by [8].

This extension has been performed at the expense of only 2 more free parameters $c_1 - c_2$ and c_3 which describe the amount by which the pure VMD assumption is violated. The precise numerical value of these are found close to the guess of Harada and Yamawaki [2] and amount to a small violation of the full VMD assumption in the Triangle Anomaly Sector and to a large violation for the Box Anomalies. On the other hand, we did not find any clear and unambiguous evidence for a high mass vector meson influence in e^+e^- annihilations up to $\simeq 1.05$ GeV.

We have also shown that all experimental data, except for a data set on $e^+e^- \rightarrow \pi^0\pi^+\pi^-$ annihilation, are successfully described by a global fit within a unified (HLS) framework. This is clearly more constraining than only accounting for partial decay widths. Systematic uncertainties, especially correlated errors, have been carefully studied because of their importance in numerical estimation of some physics parameters. It has thus been shown that all data samples have already the expected absolute scale, except for the high statistics two-pion data sample from KLOE which has to be rescaled according to expectations. Then, all e^+e^- data samples exhibit a good consistency with each other, including the KLOE sample which only marginally degrades the global fit quality.

In summary the Extended HLS Model, supplied with the vector meson mixing mechanism defined in [3] provides a successful simultaneous description of all the data falling inside its scope. One should note that this model allows for the first simultaneous fit to all the low energy data not affected by scalar mesons or higher mass vector mesons.

The last part of this study was devoted to results on partial widths of vector mesons as derived from our global fit. We have argued on the difficulty to firmly assess partial width values of vector mesons to some final state f relying only on e^+e^- annihilation to this final state. We have preferred limiting ourselves to providing our estimations for products like $\Gamma(V \rightarrow r^+e^-) \times \Gamma(V \rightarrow f)$ or ratios of the form $\Gamma(V \rightarrow f_1)/\Gamma(V \rightarrow f_2)$ where the uncertainties in estimating $\Gamma(V \rightarrow e^+e^-)$ cancel out. Taking into account the quality of our fits and the additional information provided by the physics underlying various processes, we believe our results are reliable and could supersede several older reported results.

Acknowledgements

We gratefully acknowledge, G. Venanzoni, Laboratori Nazionali di Frascati, Italy, for having provided us with the KLOE data and errors, for helpful correspondance on their handling

and for useful comments on the manuscript. We also acknowledge S. Eidelman, Budker Institute, Novosibirsk, for important information concerning CMD2 and CMD data.

Appendices

A The Non–Anomalous HLS Lagrangian

We remind [3] in this Appendix the HLS Lagrangian piece describing the photon sector (traditional VMD) :

$$\begin{aligned}
\mathcal{L}_{VMD} &= ie(1 - \frac{a}{2})A \cdot \pi^- \overleftrightarrow{\partial} \pi^+ + i\frac{e}{z_A}(z_A - \frac{a}{2} - b)A \cdot K^- \overleftrightarrow{\partial} K^+ + i\frac{e}{z_A}bA \cdot K^0 \overleftrightarrow{\partial} \overline{K}^0 \\
&+ \frac{ia g}{2}\rho_I^0 \cdot \pi^- \overleftrightarrow{\partial} \pi^+ + \frac{ia g}{4z_A}(\rho_I^0 + \omega_I - \sqrt{2}z_V\phi_I)K^- \overleftrightarrow{\partial} K^+ + \frac{ia g}{4z_A}(\rho_I^0 - \omega_I + \sqrt{2}z_V\phi_I)K^0 \overleftrightarrow{\partial} \overline{K}^0 \\
&- eagf_\pi^2 \left[\rho_I^0 + \frac{1}{3}\omega_I - \frac{\sqrt{2}}{3}z_V\phi_I \right] \cdot A + \frac{1}{9}af_\pi^2e^2(5 + z_V)A^2 + \frac{af_\pi^2g^2}{2} [(\rho_I^0)^2 + \omega_I^2 + z_V\phi_I^2]
\end{aligned} \tag{78}$$

The parameter g is the traditional universal vector meson coupling constant ; the parameter a specific of the HLS model, is expected equal to 2 in standard VMD approaches but rather fitted to $a \simeq 2.3 \div 2.5$ [63, 64, 3]. The parameter b in Eq. (78) is $b = a(z_V - 1)/6$ where z_V is the SU(3) breaking parameter of the \mathcal{L}_V part of the HLS Lagrangian, while $z_A = [f_K/f_\pi]^2 = 1.495 \pm 0.031$ [65] is the SU(3) breaking parameter of its \mathcal{L}_A part [1, 2].

A subscript I on the fields, standing for “ideal”, affects the neutral vector meson fields. It indicates that the corresponding fields occurring in the Lagrangian are not the physical fields.

On the other hand, the part of the HLS model involved in τ decays writes [3] :

$$\begin{aligned}
\mathcal{L}_\tau &= -\frac{ig_2}{2}V_{ud}W^+ \cdot \left[(1 - \frac{a}{2})\pi^- \overleftrightarrow{\partial} \pi^0 + (z_A - \frac{a}{2})\frac{1}{z_A\sqrt{2}}K^0 \overleftrightarrow{\partial} K^- \right] \\
&- \frac{af_\pi^2gg_2}{2}V_{ud}W^+ \cdot \rho^- - \frac{ia g}{2}\rho^- \left[\pi^0 \overleftrightarrow{\partial} \pi^+ - \frac{1}{z_A\sqrt{2}}\overline{K}^0 \overleftrightarrow{\partial} K^+ \right] \\
&+ f_\pi^2g_2^2 \left\{ \frac{1+a}{4} [z_A|V_{us}|^2 + |V_{ud}|^2] + \frac{a}{4}[\sqrt{z_V} - z_A]|V_{us}|^2 \right\} W^+ \cdot W^- + af_\pi^2g^2\rho^+\rho^-
\end{aligned} \tag{79}$$

plus the conjugate of the interaction term (the W^- term, not displayed). This Lagrangian piece depends on the CKM matrix element $V_{ud} = 0.97377 \pm 0.00027$ [65], on g_2 (fixed by its relation with the Fermi constant) :

$$g_2 = 2m_W \sqrt{G_F\sqrt{2}} \quad , \tag{80}$$

on the universal coupling g and on the breaking parameters z_A and z_V already defined. One should note, balancing the photon mass term in \mathcal{L}_{VMD} , a small mass term complementing the W mass of the Standard Model which could be removed by appropriate field redefinitions. At the τ lepton mass scale one has [65] :

$$g_2 = 0.629 \quad (\text{and } e = 0.30286) \quad .$$

B Effective Lagrangian Piece for $e^+e^- \rightarrow P\gamma$

The VVP Lagrangian piece relevant for the $P\gamma$ final state can be derived from the first Lagrangian in Eqs (4) ; it is given in terms of ideal fields by :

$$\begin{aligned} \mathcal{L}_{VVP} &= B\epsilon^{\mu\nu\alpha\beta} H_{\mu\nu\alpha\beta} \quad \left(B = -\frac{N_c g^2 c_3}{8\pi^2 f_\pi} \right) \\ H_{\mu\nu\alpha\beta} &= (\partial_\mu \rho_{I\nu} \partial_\alpha \rho_{I\beta} + \partial_\mu \omega_{I\nu} \partial_\alpha \omega_{I\beta}) \left[\frac{\eta_8}{2\sqrt{3}} + x \frac{\eta_0}{\sqrt{6}} \right] + \frac{z_W z_T^2}{z_A} \partial_\mu \phi_{I\nu} \partial_\alpha \phi_{I\beta} \left[\frac{-\eta_8}{\sqrt{3}} + x \frac{\eta_0}{\sqrt{6}} \right] \\ &\quad + \partial_\mu \rho_{I\nu} \partial_\alpha \omega_{I\beta} \pi^0 \end{aligned} \quad (81)$$

where the pseudoscalar fields are still the bare fields.

As stated in the main text, the condition $z_W z_T^2 = 1$ is requested. Using this piece and Eq. (78), one can define an equivalent effective term which allows for a simpler derivation of the $VP\gamma$ couplings :

$$\mathcal{L}'_{AVP} = B' \epsilon^{\mu\nu\alpha\beta} \text{Tr} \left[\partial_\mu (eQA_\nu + gc_3 V_\nu) \partial_\alpha (eQA_\beta + gc_3 V_\beta) X_A^{-1/2} (P_8 + xP_0) X_A^{-1/2} \right] \quad (82)$$

where now the pseudoscalar fields are the renormalized ones, Q is the quark charge matrix, A is the electromagnetic field and B' is given below. The effective piece of interest can further be written :

$$\left\{ \begin{aligned} \mathcal{L}'_{AVP} &= B' \epsilon^{\mu\nu\alpha\beta} \partial_\mu A_\nu H_{\alpha\beta} \quad \left(\text{with } B' = -\frac{N_c e g c_3}{4\pi^2 f_\pi} \right) \\ H_{\alpha\beta} &= \partial_\alpha \rho_\beta^I \left[\frac{\pi^0}{6} + \frac{\eta_8}{2\sqrt{3}} + \frac{x\eta_0}{\sqrt{6}} \right] + \partial_\alpha \omega_\beta^I \left[\frac{\pi^0}{2} + \frac{\eta_8}{6\sqrt{3}} + \frac{x\eta_0}{3\sqrt{6}} \right] \\ &\quad + \partial_\alpha \phi_\beta^I \frac{1}{3z_A} \left[\sqrt{\frac{2}{3}} \eta_8 - \frac{x}{\sqrt{3}} \eta_0 \right] \end{aligned} \right. \quad (83)$$

in terms of renormalized ideal and pseudoscalar fields, renormalized after applying the SU(3)/U(3) breaking mechanism. One can now replace the ideal vector fields by their physical partners using Eqs. (22) and gets :

$$\mathcal{L}'_{AVP} = B' \sum_{i,j} H_{V_i}^{P_j} P_j \epsilon^{\mu\nu\alpha\beta} \partial_\mu A_\nu \partial_\alpha V_{i\beta} \quad (84)$$

where the sum extends over the physical (neutral) vector fields and the neutral pseudoscalar mesons. We have defined ($\Lambda = \sqrt{2}/z_A$) :

$$\left\{ \begin{aligned} H_\rho^{\pi^0} &= \frac{1+3\alpha}{6}, & H_\omega^{\pi^0} &= \frac{3-\alpha}{6}, & H_\phi^{\pi^0} &= \frac{\beta+3\gamma}{6} \\ H_\rho^{\eta_8} &= \frac{3+\alpha-2\Lambda\beta}{6\sqrt{3}}, & H_\omega^{\eta_8} &= \frac{1-3\alpha-2\Lambda\gamma}{6\sqrt{3}}, & H_\phi^{\eta_8} &= \frac{\gamma+3\beta+2\Lambda}{6\sqrt{3}} \\ H_\rho^{\eta_0} &= x \frac{3+\alpha+\Lambda\beta}{3\sqrt{6}}, & H_\omega^{\eta_0} &= x \frac{1-3\alpha+\Lambda\gamma}{3\sqrt{6}}, & H_\phi^{\eta_0} &= x \frac{3\beta+\gamma-\Lambda}{3\sqrt{6}} \end{aligned} \right. \quad (85)$$

where the dependence of the "angles" upon s has been omitted.

The other Lagrangian piece contributing to $e^+e^- \rightarrow P\gamma$ annihilations is (see Eqs. (4) :

$$\begin{cases} \mathcal{L}_{AAP} = B'' \epsilon^{\mu\nu\alpha\beta} \partial_\mu A_\nu \partial_\alpha A_\beta K \quad , & \left(B'' = -\frac{e^2 N_c}{4\pi^2 f_\pi} (1 - c_3) \right) \\ K = \left[\frac{\pi^0}{6} + \frac{5z_A - 2}{3z_A} \frac{\eta_8}{6\sqrt{3}} + \frac{5z_A + 1}{3z_A} \frac{x}{3} \frac{\eta_0}{\sqrt{6}} \right] \end{cases} \quad (86)$$

which provides the constant contributions to the amplitudes given by Eqs. (41).

C Integrated Cross Section For $e^+e^- \rightarrow \pi^+\pi^-\pi^0$

Using the parametrization of Kuraev and Siligadze [43], the differential cross section is written :

$$\frac{d^2\sigma(e^+e^- \rightarrow \pi^+\pi^-\pi^0)}{dx dy} = \frac{\alpha_{em}}{192\pi^2} s^2 G(x, y) |T_{sym} + T_\rho|^2 \quad (87)$$

where :

$$G(x, y) = 4\left(x^2 - \frac{m_\pi^2}{s}\right)\left(y^2 - \frac{m_\pi^2}{s}\right) - \left(1 - 2x - 2y + 2xy + \frac{2m_\pi^2 - m_0^2}{s}\right)^2 \quad (88)$$

The variables x and y are defined by ($m_0 = m_{\pi^0}$, $m_\pi = m_{\pi^\pm}$) by :

$$\begin{cases} s_{+-} = s(2x + 2y - 1) + m_0^2 \\ s_{+0} = s(1 - 2y) + m_\pi^2 \\ s_{-0} = s(1 - 2x) + m_\pi^2 \end{cases} \quad (89)$$

The integrated cross section is :

$$\sigma(e^+e^- \rightarrow \pi^+\pi^-\pi^0) = \int_{x_{min}}^{x_{max}} dx \int_{y_{min}}^{y_{max}} dy \frac{d^2\sigma(e^+e^- \rightarrow \pi^+\pi^-\pi^0)}{dx dy} \quad (90)$$

with :

$$\begin{cases} x_{min} = \frac{m_\pi}{\sqrt{s}} \quad , \quad x_{max} = \frac{1}{2} \left(1 - \frac{m_0(2m_\pi + m_0)}{s} \right) \\ y_{min/max} = \frac{1}{2(1 - 2x + x_{min}^2)} \left\{ (1 - x)(1 - 2x + \frac{(2m_\pi^2 - m_0^2)}{s}) \right. \\ \left. +/ - \left[\left(x^2 - \frac{m_\pi^2}{s} \right) (1 - 2x + \frac{m_0(2m_\pi - m_0)}{s}) \left(1 - 2x - \frac{m_0(2m_\pi + m_0)}{s} \right) \right]^{1/2} \right\} \end{cases} \quad (91)$$

References

- [1] M. Bando, T. Kugo, and K. Yamawaki, Phys. Rept. **164**, 217 (1988), Nonlinear Realization and Hidden Local Symmetries.
- [2] M. Harada and K. Yamawaki, Phys. Rept. **381**, 1 (2003), hep-ph/0302103, Hidden local symmetry at loop: A new perspective of composite gauge boson and chiral phase transition.
- [3] M. Benayoun, P. David, L. DelBuono, O. Leitner, and H. B. O'Connell, Eur. Phys. J. **C55**, 199 (2008), hep-ph/0711.4482, The Dipion Mass Spectrum In e^+e^- Annihilation and tau Decay: A Dynamical (ρ^0, ω, ϕ) Mixing Approach.
- [4] M. Benayoun and H. B. O'Connell, Phys. Rev. **D58**, 074006 (1998), hep-ph/9804391, SU(3) breaking and hidden local symmetry.
- [5] M. Benayoun, L. DelBuono, S. Eidelman, V. N. Ivanchenko, and H. B. O'Connell, Phys. Rev. **D59**, 114027 (1999), hep-ph/9902326, Radiative decays, nonet symmetry and SU(3) breaking.
- [6] M. Bando, T. Kugo, and K. Yamawaki, Nucl. Phys. **B259**, 493 (1985), On the Vector Mesons as Dynamical Gauge Bosons of Hidden Local Symmetries.
- [7] T. Fujiwara, T. Kugo, H. Terao, S. Uehara, and K. Yamawaki, Prog. Theor. Phys. **73**, 926 (1985), Nonabelian Anomaly and Vector Mesons as Dynamical Gauge Bosons of Hidden Local Symmetries.
- [8] A. Bramon, R. Escribano, J. L. L. M., and G. Pancheri, Phys. Lett. **B486**, 406 (2000), hep-ph/0003273, The ratio $\phi \rightarrow K^+K^-/K^0\bar{K}^0$.
- [9] S. Dubynskiy, A. Le Yaouanc, L. Oliver, J. C. Raynal, and M. B. Voloshin, Phys. Rev. **D75**, 113001 (2007), arXiv:0704.0293 [hep-ph], Isospin breaking in the yield of heavy meson pairs in e^+e^- annihilation near threshold.
- [10] J. Wess and B. Zumino, Phys. Lett. **B37**, 95 (1971), Consequences of anomalous Ward identities.
- [11] E. Witten, Nucl. Phys. **B223**, 422 (1983), Global Aspects of Current Algebra.
- [12] KLOE, A. Aloisio *et al.*, Phys. Lett. **B606**, 12 (2005), hep-ex/0407048, Measurement of $\sigma(e^+e^- \rightarrow \pi^+\pi^-\gamma)$ and extraction of $\sigma(e^+e^- \rightarrow \pi^+\pi^-)$ below 1-GeV with the KLOE detector.
- [13] KLOE, F. Ambrosino *et al.*, Phys. Lett. **B670**, 285 (2009), 0809.3950, Measurement of $\sigma(e^+e^- \rightarrow \pi^+\pi^-\gamma(\gamma))$ and the dipion contribution to the muon anomaly with the KLOE detector.
- [14] M. Benayoun, P. David, L. DelBuono, P. Leruste, and H. B. O'Connell, Eur. Phys. J. **C31**, 525 (2003), nucl-th/0306078, Anomalous η/η' decays: The triangle and box anomalies.

- [15] M. Benayoun, L. DelBuono, and H. B. O'Connell, Eur. Phys. J. **C17**, 593 (2000), hep-ph/9905350, VMD, the WZW Lagrangian and ChPT: The third mixing angle.
- [16] G. 't Hooft, Phys. Rept. **142**, 357 (1986), How Instantons Solve the U(1) Problem.
- [17] A. Bramon, A. Grau, and G. Pancheri, Phys. Lett. **B345**, 263 (1995), hep-ph/9411269, Effective chiral lagrangians with an SU(3) broken vector meson sector.
- [18] A. Bramon, A. Grau, and G. Pancheri, Phys. Lett. **B344**, 240 (1995), Radiative vector meson decays in SU(3) broken effective chiral Lagrangians.
- [19] Particle Data Group, c. Amsler *et al.*, Phys. Lett. **B667**, 1 (2008), Review of particle physics.
- [20] L. M. Barkov *et al.*, Nucl. Phys. **B256**, 365 (1985), Electromagnetic Pion Form-Factor in the Timelike Region.
- [21] A. Quenzer *et al.*, Phys. Lett. **B76**, 512 (1978), Pion Form-Factor from 480-MeV to 1100-MeV.
- [22] CMD-2, A. V. M. others, Phys. Lett. **B527**, 161 (2002), hep-ex/0112031, Measurement of $e^+e^- \rightarrow \pi^+\pi^-$ cross section with CMD-2 around rho meson.
- [23] CMD-2, R. R. Akhmetshin *et al.*, Phys. Lett. **B578**, 285 (2004), hep-ex/0308008, Re-analysis of hadronic cross section measurements at CMD- 2.
- [24] CMD-2, R. R. Akhmetshin *et al.*, Phys. Lett. **B648**, 28 (2007), hep-ex/0610021, High-statistics measurement of the pion form factor in the rho-meson energy range with the CMD-2 detector.
- [25] R. R. Akhmetshin *et al.*, JETP Lett. **84**, 413 (2006), hep-ex/0610016, Measurement of the $e^+e^- \rightarrow \pi^+\pi^-$ cross section with the CMD-2 detector in the 370-MeV - 520-MeV cm energy range.
- [26] M. N. Achasov *et al.*, J. Exp. Theor. Phys. **103**, 380 (2006), hep-ex/0605013, Update of the $e^+e^- \rightarrow \pi^+\pi^-$ cross section measured by SND detector in the energy region 400-MeV $< \sqrt{s} < 1000$ -MeV.
- [27] S. Eidelman, private communication .
- [28] F. Jegerlehner, www-com.physik.hu-berlin.de/fjeger/.
- [29] A. Hofer, J. Gluza, and F. Jegerlehner, Eur. Phys. J. **C24**, 51 (2002), hep-ph/0107154, Pion pair production with higher order radiative corrections in low energy e^+e^- collisions.
- [30] F. Jegerlehner, Acta Phys. Polon. **B38**, 3021 (2007), hep-ph/0703125, Essentials of the Muon g-2.
- [31] F. Jegerlehner, Nucl. Phys. Proc. Suppl. **131**, 213 (2004), hep-ph/0312372, The role of $\sigma(e^+e^- \rightarrow \text{hadrons})$ in precision tests of the standard model.

- [32] F. Jegerlehner, Nucl. Phys. Proc. Suppl. **126**, 325 (2004), hep-ph/0310234, Theoretical precision in estimates of the hadronic contributions to $(g - 2)_\mu$ and $\alpha(\text{QED})(M(Z))$.
- [33] NA7, S. R. Amendolia *et al.*, Nucl. Phys. **B277**, 168 (1986), A Measurement of the Space - Like Pion Electromagnetic Form-Factor.
- [34] E. B. Dally *et al.*, Phys. Rev. Lett. **48**, 375 (1982), Elastic Scattering Measurement of the Negative Pion Radius.
- [35] KLOE, F. Ambrosino *et al.*, Phys. Lett. **B648**, 267 (2007), hep-ex/0612029, Measurement of the pseudoscalar mixing angle and eta' gluonium content with KLOE detector.
- [36] CMD2, R. R. Akhmetshin *et al.*, Phys. Lett. **B605**, 26 (2005), hep-ex/0409030, Study of the Processes $e^+e^- \rightarrow \eta\gamma$, $e^+e^- \rightarrow \pi^0\gamma \rightarrow 3\gamma$ in the c.m. Energy Range 600–1380 MeV at CMD-2.
- [37] CMD2, R. R. Akhmetshin *et al.*, Phys. Lett. **B460**, 242 (1999), hep-ex/9907003, Study of the radiative decay $\phi \rightarrow \eta\gamma$ with CMD-2 detector.
- [38] M. N. Achasov *et al.*, Phys. Rev. **D76**, 077101 (2007), 0709.1007, Reanalysis of the $e^+e^- \rightarrow \eta\gamma$ reaction cross section.
- [39] M. N. Achasov *et al.*, Phys. Lett. **B559**, 171 (2003), hep-ex/0302004, Experimental study of the $e^+e^- \rightarrow \pi^0\gamma$ process in the energy region $\sqrt{s} = 0.60 - 0.97$ GeV.
- [40] M. N. Achasov *et al.*, Eur. Phys. J. **C12**, 25 (2000), Experimental study of the processes $e^+e^- \rightarrow \phi \rightarrow \eta\gamma, \pi^0\gamma$ at VEPP-2M.
- [41] KLOE, Müller. *et al.*, KLOE Note **221** (2008), www.inf.it/kloe/pub/knote/kn221.pdf, Measurement of $\sigma(e^+e^- \rightarrow \pi^+\pi^-\gamma(\gamma))$ and the dipion contribution to the muon anomaly with the KLOE detector.
- [42] G. Venanzoni, private communication .
- [43] E. A. Kuraev and Z. K. Silagadze, Phys. Atom. Nucl. **58**, 1589 (1995), hep-ph/9502406, Once more about the $\omega \rightarrow \pi\pi\pi$ contact term.
- [44] R. R. Akhmetshin *et al.*, Phys. Lett. **B364**, 199 (1995), Measurement of phi meson parameters with CMD-2 detector at VEPP-2M collider.
- [45] R. R. Akhmetshin *et al.*, Phys. Lett. **B434**, 426 (1998), Study of dynamics of $\phi \rightarrow \pi^+\pi^-\pi^0$ decay with CMD-2 detector.
- [46] R. R. Akhmetshin *et al.*, Phys. Lett. **B642**, 203 (2006), Study of $\phi \rightarrow \pi^+\pi^-\pi^0$ with CMD-2 detector.
- [47] M. N. Achasov *et al.*, Phys. Rev. **D68**, 052006 (2003), hep-ex/0305049, Study of the process $e^+e^- \rightarrow \pi^+\pi^-\pi^0$ in the energy region \sqrt{s} below 0.98 GeV.
- [48] M. N. Achasov *et al.*, Phys. Rev. **D66**, 032001 (2002), hep-ex/0201040, Study of the process $e^+e^- \rightarrow \pi^+\pi^-\pi^0$ in the energy region \sqrt{s} from 0.98 to 1.38 GeV.

- [49] A. Cordier *et al.*, Nucl. Phys. **B172**, 13 (1980), Cross-section of the reaction $e^+e^- \rightarrow \pi^+\pi^-\pi^0$ for center-of-mass energies from 750-MeV to 1100-MeV.
- [50] CMD, L. M. Barkov *et al.*, (1989), BudkerINP preprint 89-15, Novosibirsk.
- [51] S. I. Dolinsky *et al.*, Phys. Rept. **202**, 99 (1991), Summary of experiments with the neutral detector at the e^+e^- storage ring VEPP-2M.
- [52] M. Gormley *et al.*, Phys. Rev. **D2**, 501 (1970), Experimental determination of the dalitz-plot distribution of the decays $\eta \rightarrow \pi^+\pi^-\pi^0$ and $\eta \rightarrow \pi^+\pi^-\gamma$, and the branching ratio $\eta \rightarrow \pi^+\pi^-\gamma$.
- [53] J. G. Layter *et al.*, Phys. Rev. **D7**, 2565 (1973), Study of dalitz-plot distributions of the decays $\eta \rightarrow \pi^+\pi^-\pi^0$ and $\eta \rightarrow \pi^+\pi^-\gamma$.
- [54] A. Grigorian *et al.*, Nucl. Phys. **B91**, 232 (1975), Charge Conjugation invariance in $\eta'(959) \rightarrow \pi^+\pi^-\gamma$.
- [55] TASSO, M. Althoff *et al.*, Phys. Lett. **B147**, 487 (1984), Measurement of the radiative width of the $\eta'(958)$ in two photon interactions.
- [56] ARGUS, H. Albrecht *et al.*, Phys. Lett. **B199**, 457 (1987), Measurement of $\eta' \rightarrow \pi^+\pi^-\gamma$ in $\gamma\gamma$ collisions.
- [57] TPC/Two Gamma, H. Aihara *et al.*, Phys. Rev. **D35**, 2650 (1987), Study of η' formation gamma in $\gamma\gamma$ collisions.
- [58] Lepton F, S. I. Bityukov *et al.*, Z. Phys. **C50**, 451 (1991), Study of the radiative decay $\eta' \rightarrow \pi^+\pi^-\gamma$.
- [59] Crystal Barrel, A. Abele *et al.*, Phys. Lett. **B402**, 195 (1997), Measurement of the decay distribution of $\eta' \rightarrow \pi^+\pi^-\pi^-\gamma$ and evidence for the box anomaly.
- [60] M. Harada and K. Yamawaki, Phys. Rev. **D64**, 014023 (2001), hep-ph/0009163, Wilsonian matching of effective field theory with underlying QCD.
- [61] M. Benayoun, P. David, L. DelBuono, and Leitner, Submitted to Eur. Phys. J. , hep-ph/yymm.xxxx, A Global Treatment of VMD Physics Up to To the ϕ : I. e^+e^- Annihilations and Anomalies.
- [62] KLOE, F. Ambrosino *et al.*, Phys. Lett. **B608**, 199 (2005), hep-ex/0411082, Measurement of the leptonic decay widths of the Phi-meson with the KLOE detector.
- [63] M. Benayoun *et al.*, Eur. Phys. J. **C2**, 269 (1998), hep-ph/9707509, New results in ρ^0 meson physics.
- [64] M. Benayoun, P. David, L. DelBuono, P. Leruste, and H. B. O'Connell, Eur. Phys. J. **C29**, 397 (2003), nucl-th/0301037, The pion form factor within the Hidden Local Symmetry model.

- [65] Particle Data Group, W. M. Yao *et al.*, J. Phys. **G33**, 1 (2006), Review of particle physics.
- [66] CMD-2, R. R. Akhmetshin *et al.*, Phys. Lett. **B509**, 217 (2001), hep-ex/0103043, Study of the Process $e^+e^- \rightarrow \eta\gamma$ in c.m. Energy Range 600-1380 MeV at CMD-2.

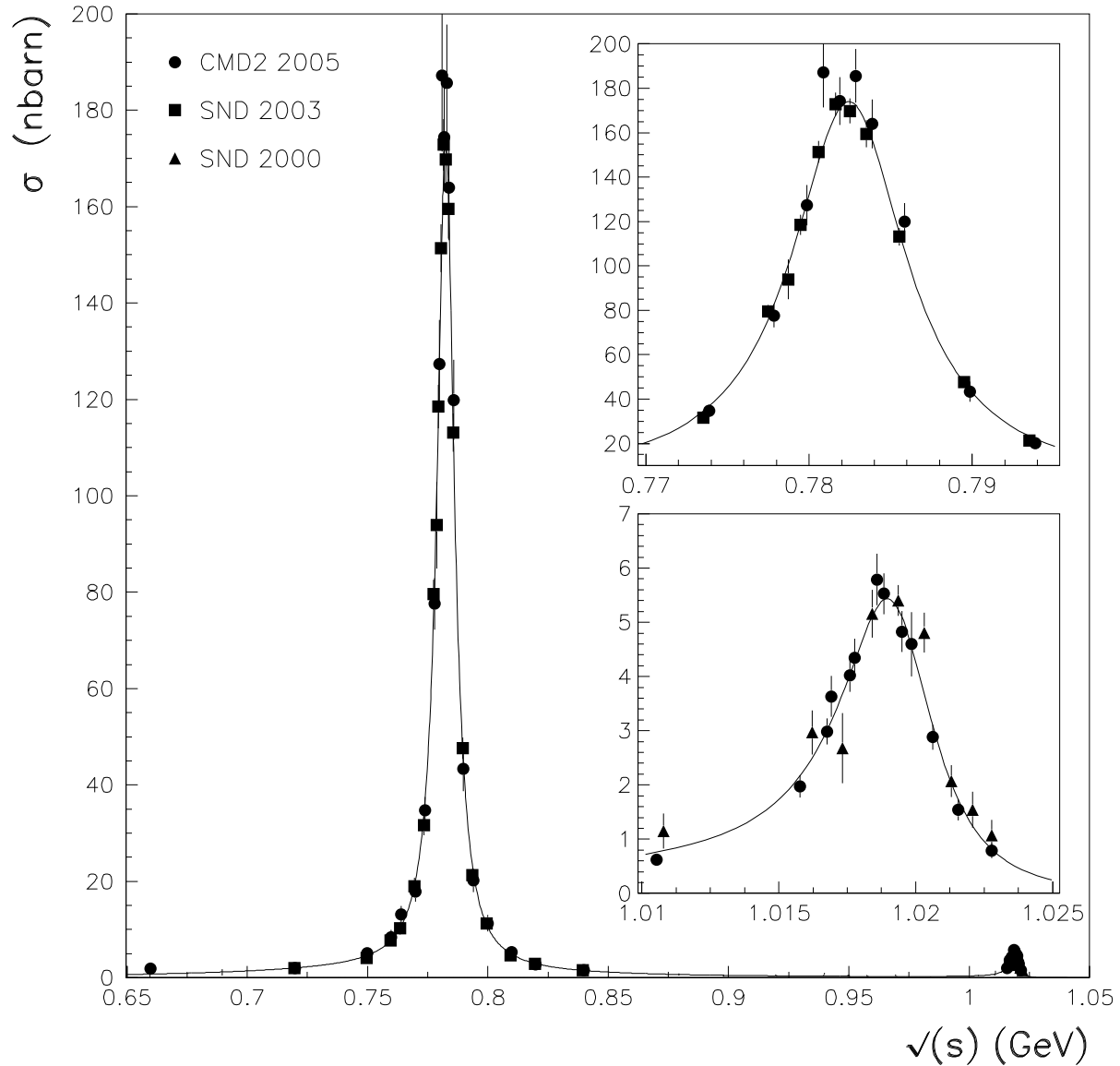


Figure 1: Annihilation process $e^+e^- \rightarrow \pi^0\gamma$. The errors plotted combine the reported systematic and statistical errors in quadrature. The insets magnify the top part of the ω region on the one hand and the ϕ region on the other hand. "CMD-2 2005" refers to [36], "SND 2003" to [39] and "SND 2000" to [40].

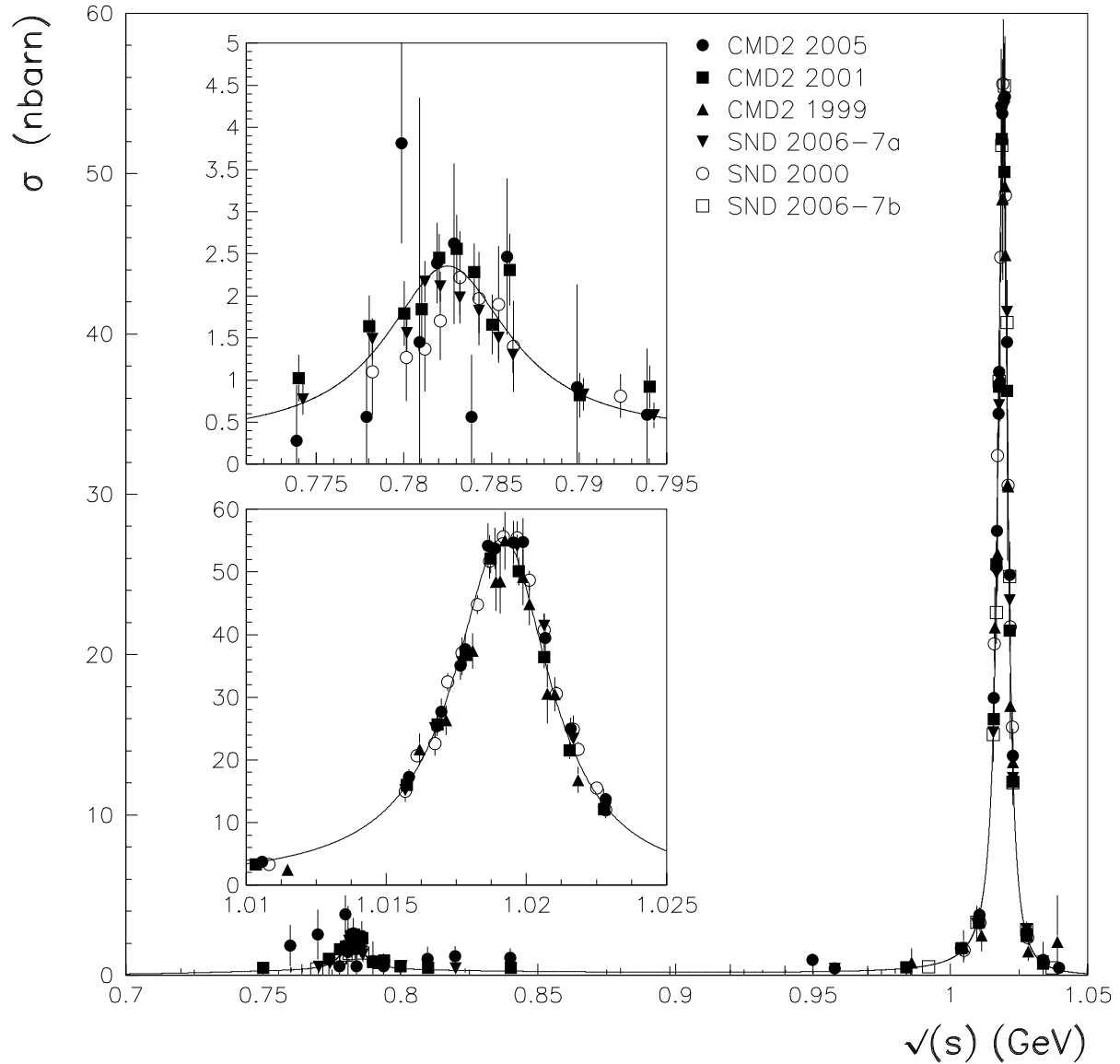


Figure 2: Annihilation process $e^+e^- \rightarrow \eta\gamma$. The errors plotted combine the reported systematic and statistical errors in quadrature. The insets magnify the ω region and the ϕ region. "CMD-2 2005" refers to [36] (with $\eta \rightarrow 2\gamma$), "CMD-2 2001" to [66] (with $\eta \rightarrow 3\pi^0$), "CMD-2 1999" to [37] (with $\eta \rightarrow \pi^+\pi^-\pi^0$), "SND 2006-7a/b" refer to the two data sets published in [38] (with $\eta \rightarrow 3\pi^0$ and $\eta \rightarrow \pi^+\pi^-\pi^0$) and "SND 2000" to the data set published in [40] (with $\eta \rightarrow 2\gamma$).

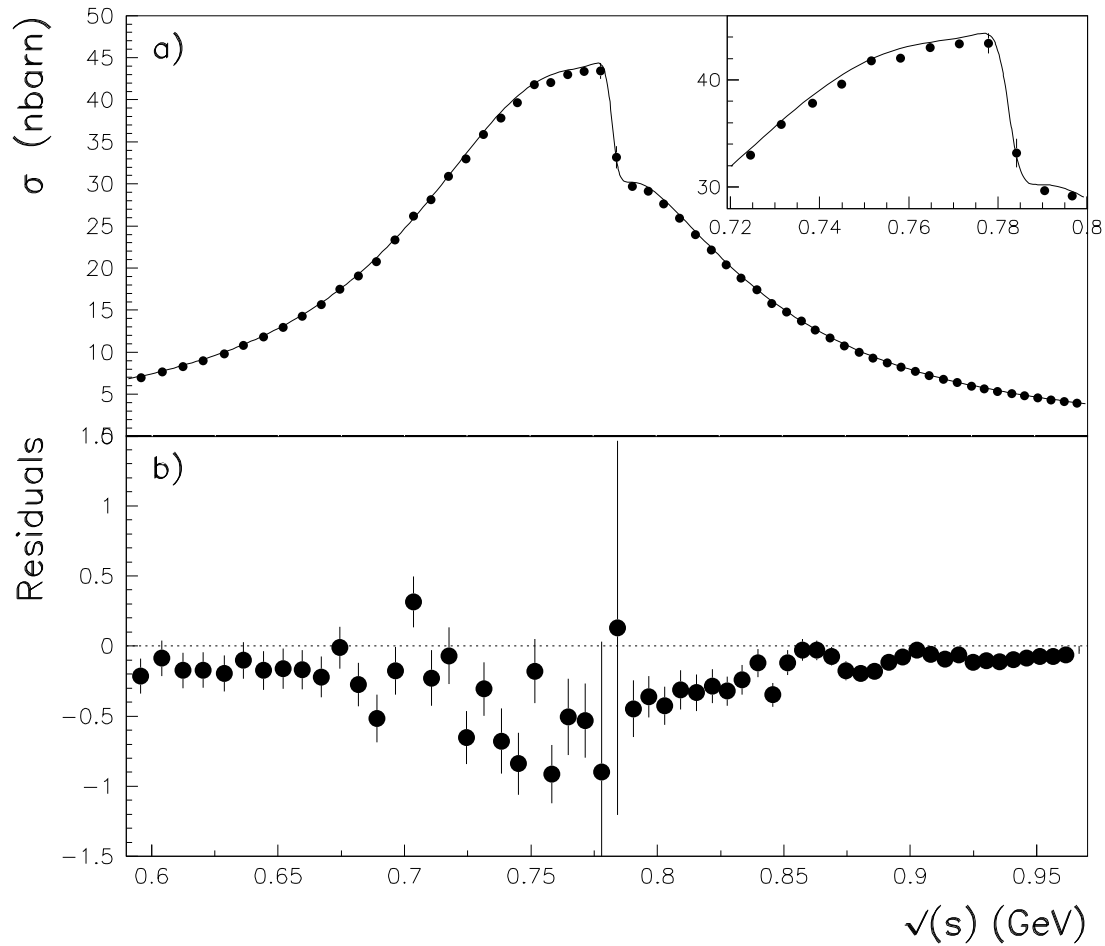


Figure 3: ISR data [13] on the $e^+e^- \rightarrow \pi^+\pi^-$ cross section collected by the KLOE Collaboration at DAΦNE with the fit superimposed. The plotted errors are the square roots of the diagonal terms in the full error covariance matrix (see text). The inset magnifies the $\rho - \omega$ region. Downmost plot shows the residual spectrum (with same units) coming out from the global fit performed with all Novosibirsk $e^+e^- \rightarrow \pi^+\pi^-$ and $e^+e^- \rightarrow (\pi^0/\eta)\gamma$ data.

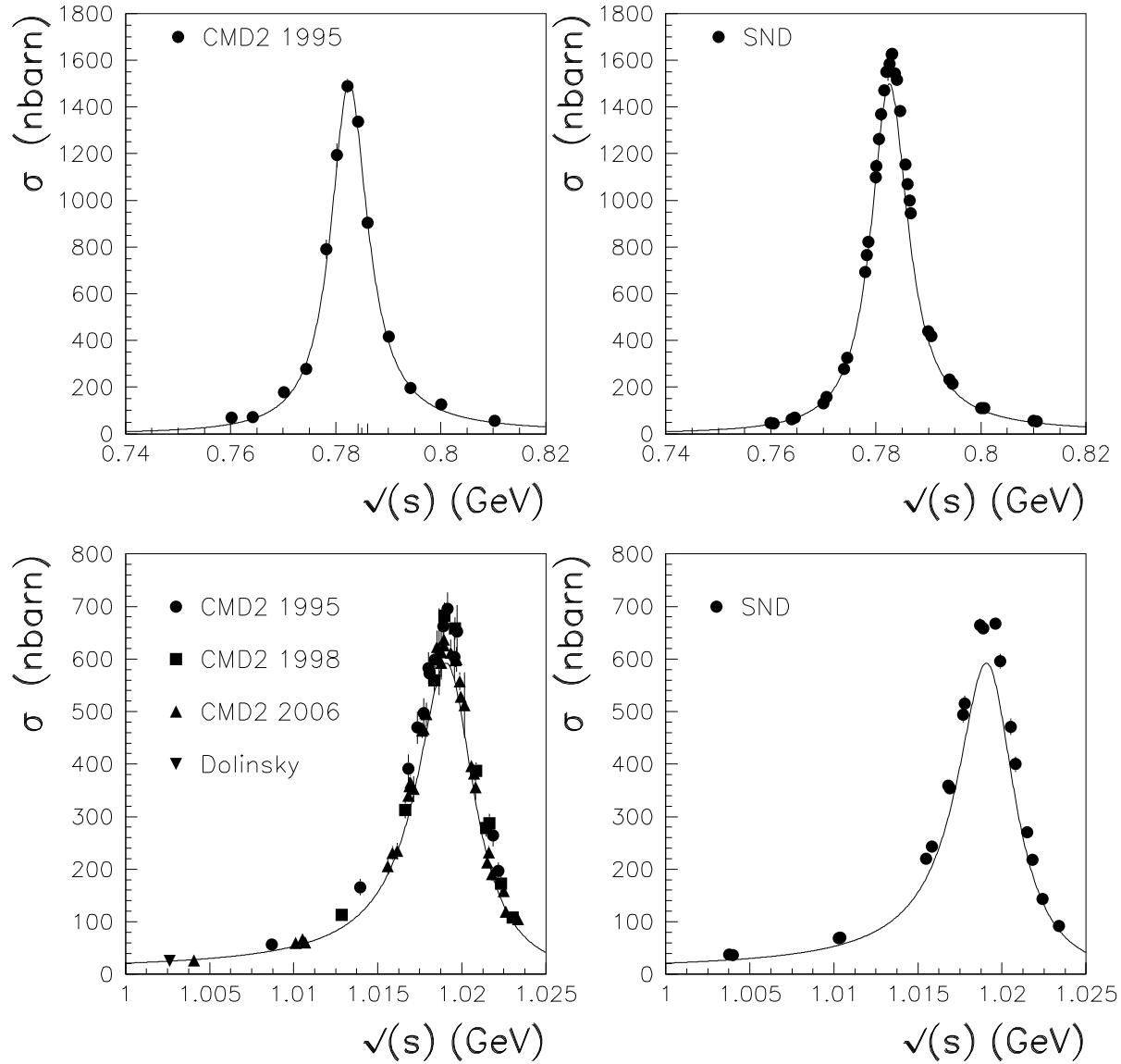


Figure 4: Plots of CMD-2 data (left figures) and SND data (right figures) superimposed with the cross section predicted from running the global fit with the ND and CMD data as single 3-pion data sets. Top figures show the case in the ω peak region, downmost figures show the ϕ peak region. See text for reference and comments.

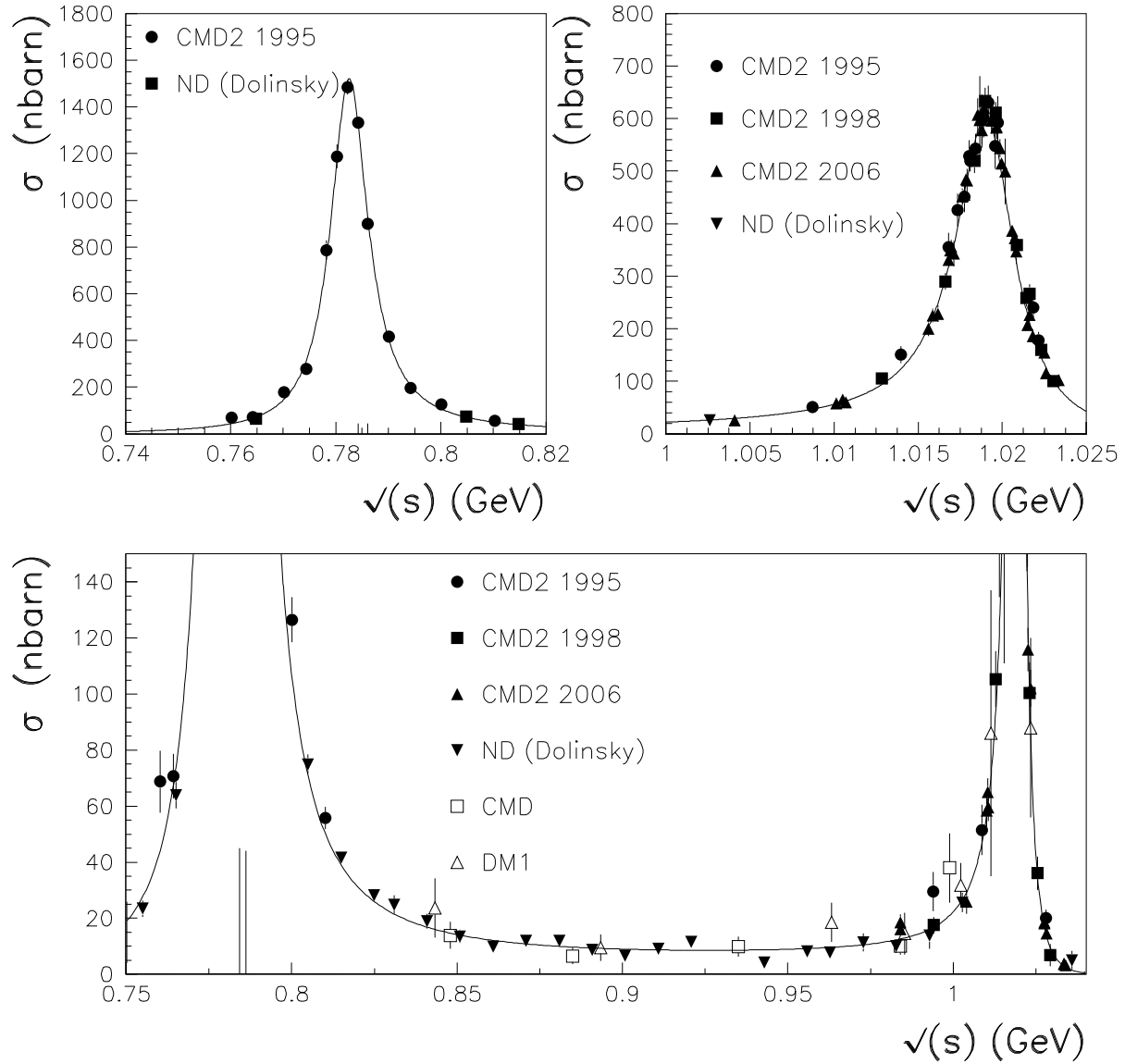


Figure 5: Fit performed using CMD–2, ND and the old CMD data (see text). Top figures show the ω and ϕ peak regions, the downmost plot shows, magnified, the region outside the peaks. The measurements of the former DM1 data set have not been used in the fit, but are nevertheless displayed in this plot. See text for references and comments.

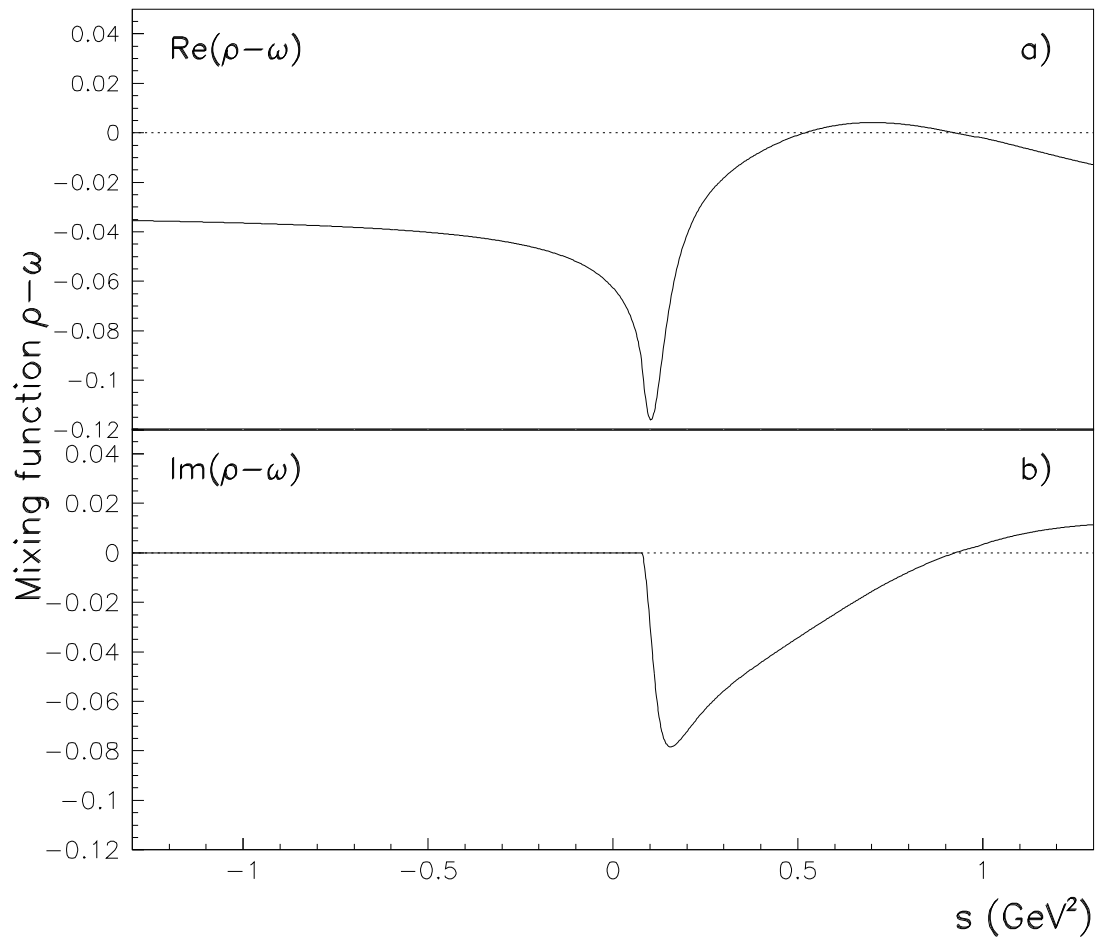


Figure 6: The isospin breaking parameter $\alpha(s)$.

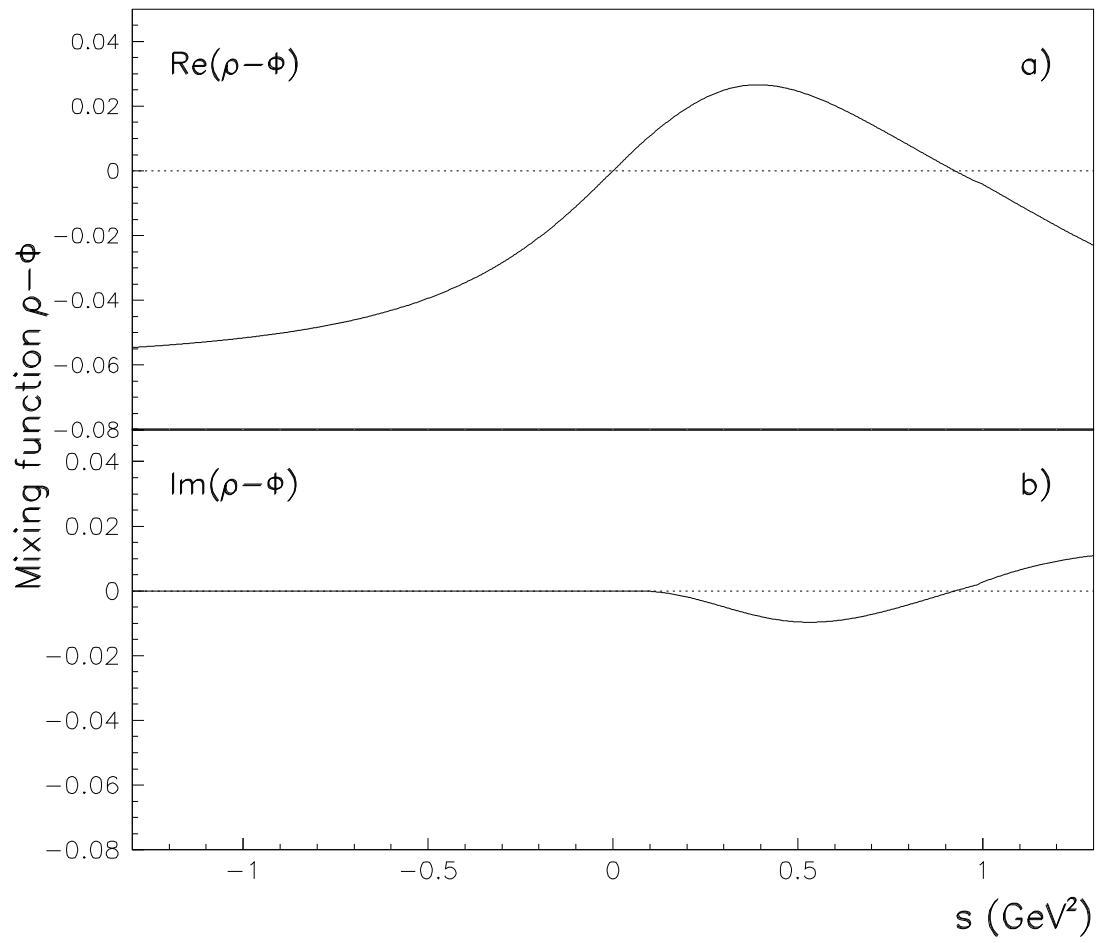


Figure 7: The isospin breaking parameter $\beta(s)$.

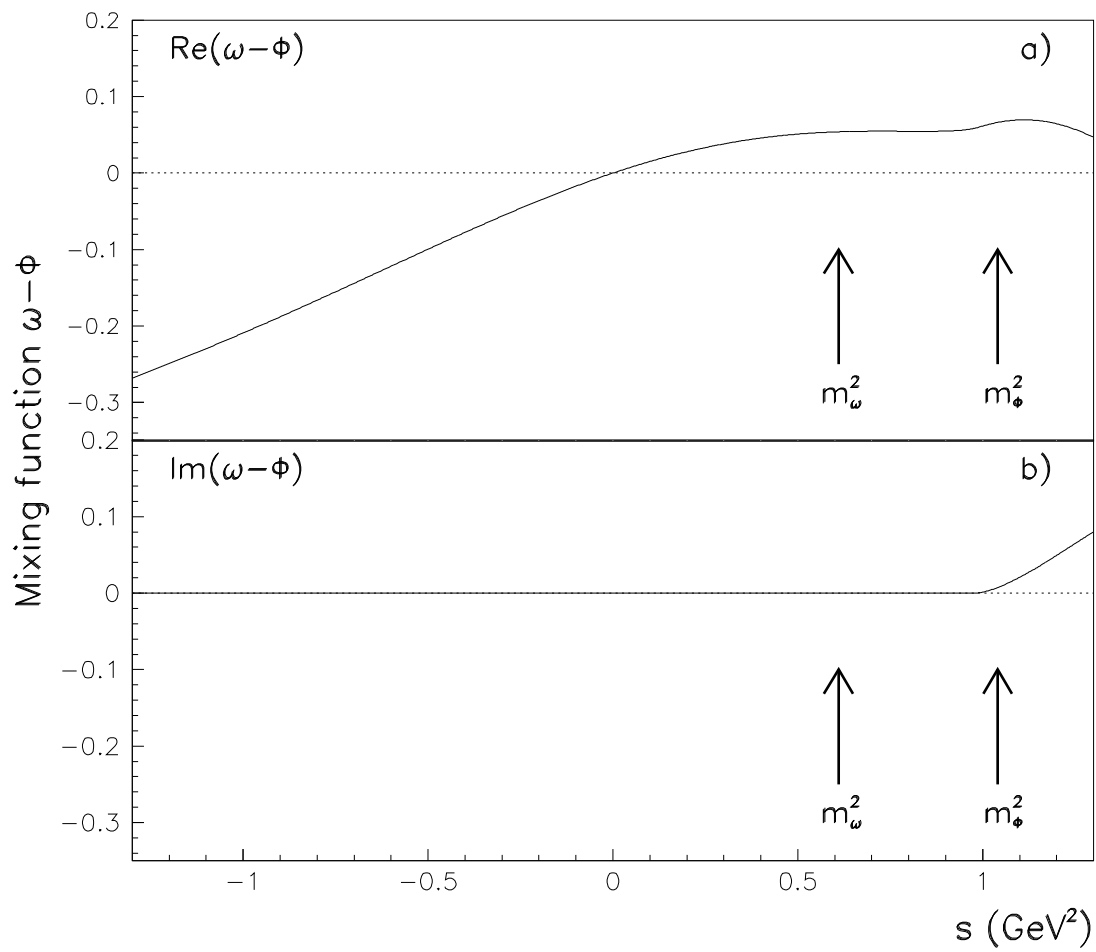


Figure 8: The isospin breaking parameter $\gamma(s)$.

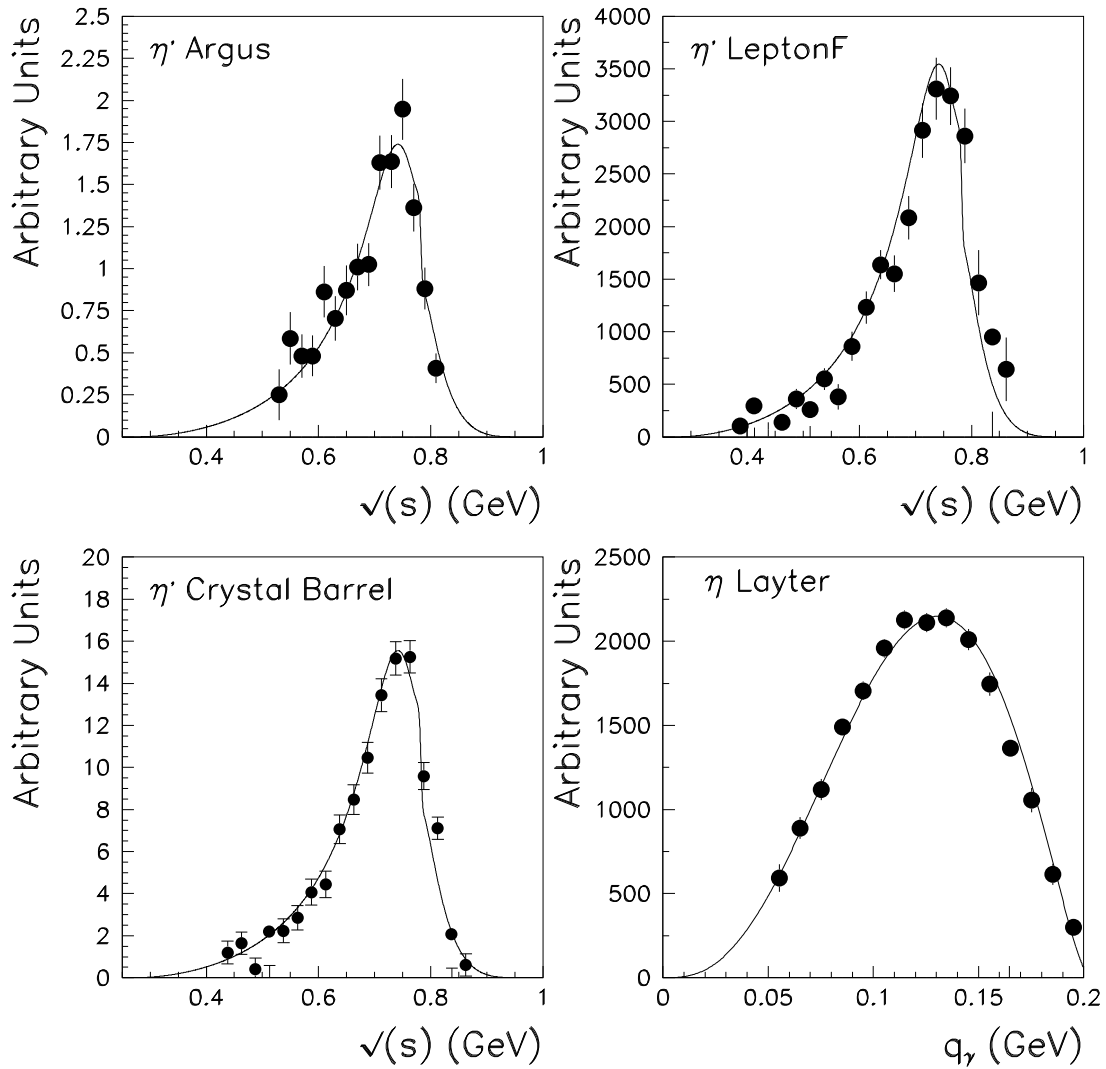


Figure 9: Dipion invariant mass spectra in the $\eta' \rightarrow \pi^+\pi^-\gamma$ decays from Argus [56], Lepton F [58] and Crystal Barrel [59] experiments. The last plot shows the photon momentum spectrum in the decay $\eta \rightarrow \pi^+\pi^-\gamma$ from [53]. The curves superimposed are predictions, not fits.

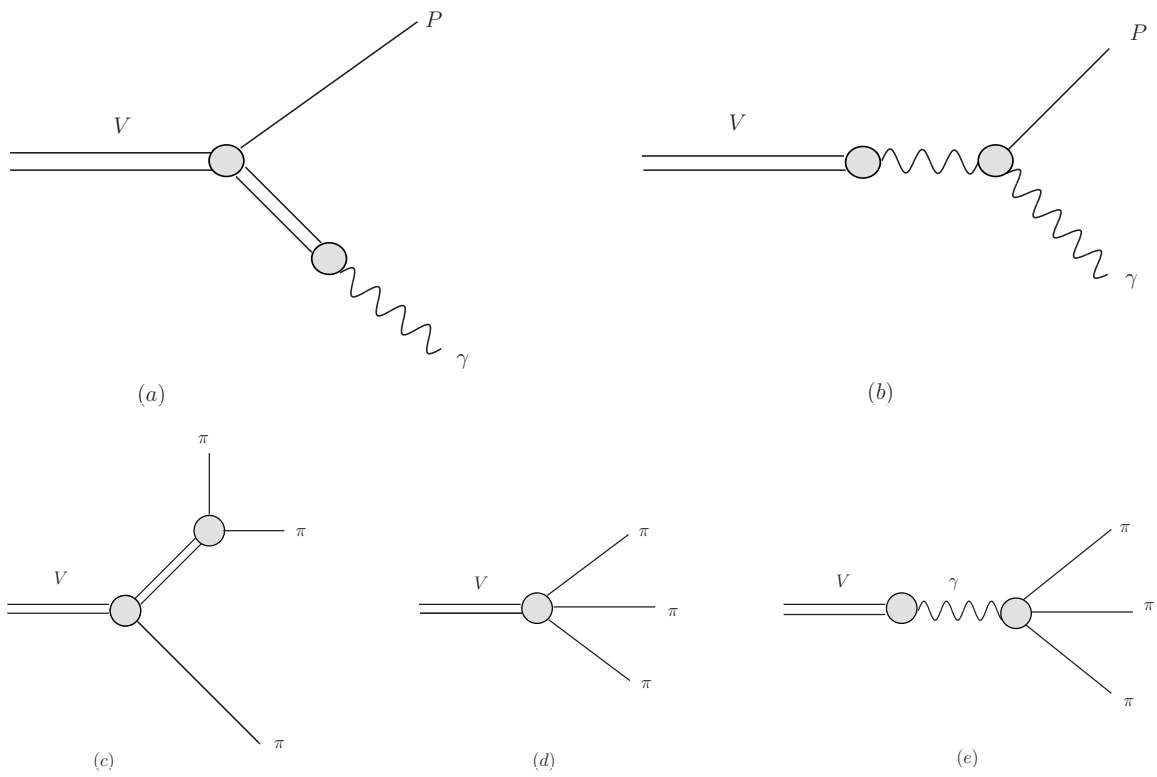


Figure 10: Diagrams sketching the contributions to radiative decays – (a) and (b)– and to three pion decays – (c), (d), (e)– of vector mesons.